Fourth International Workshop on

VALIDATION OF COMPUTATIONAL MECHANICS MODELS

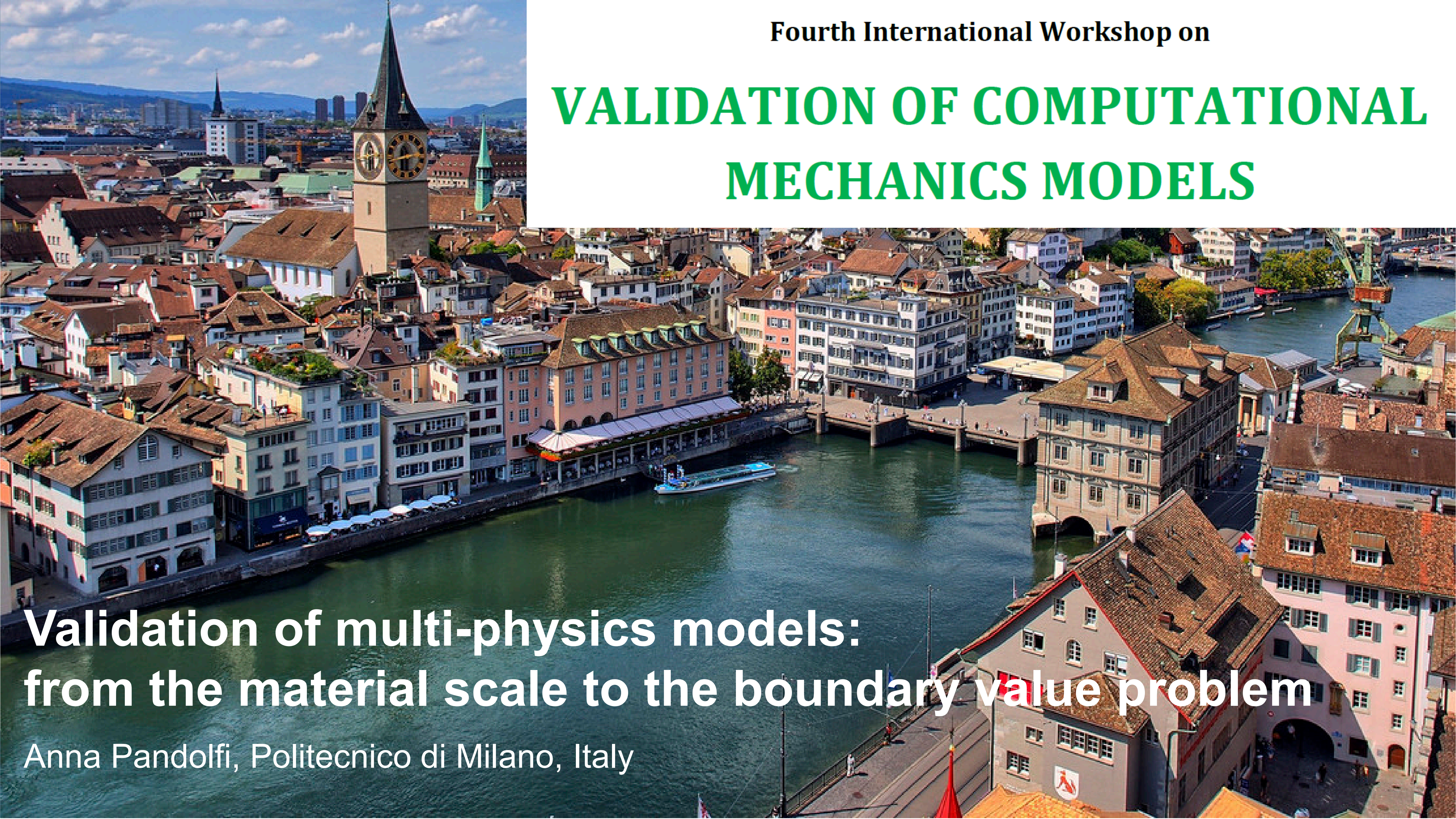

Validation of multi-physics models: from the material scale to the boundary value problem

Anna Pandolfi, Politecnico di Milano, Italy

Multi-physics & Multi-scale Challenges in Computational Mechanics

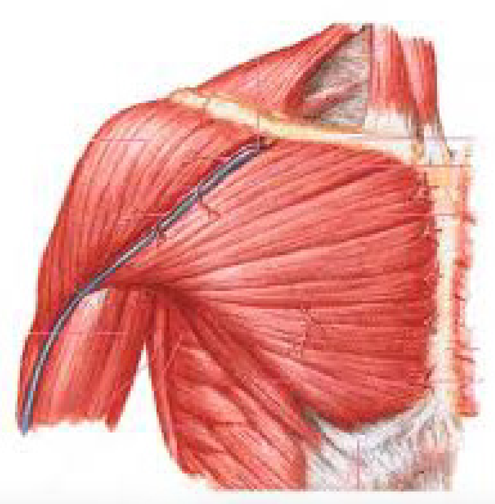

Two representative examples

- Faults and fractures permeated of water in geomechanical materials
- Collagen fiber architecture and electric activity in biological tissues

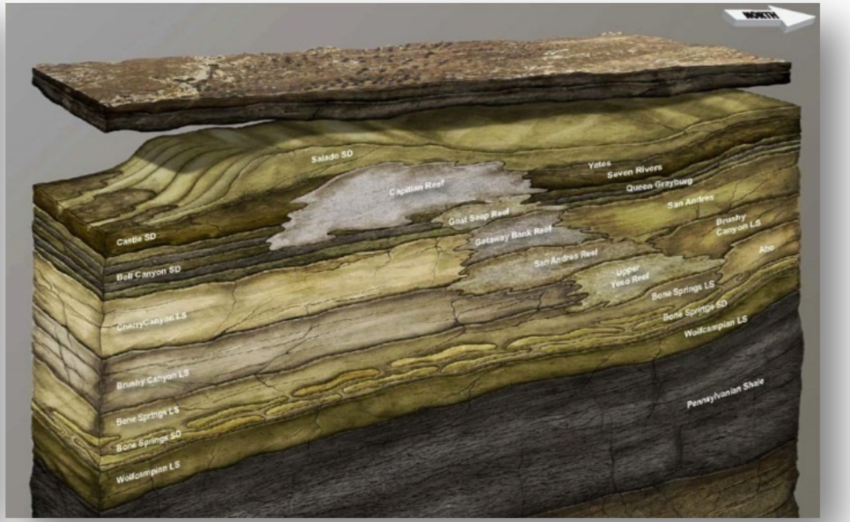

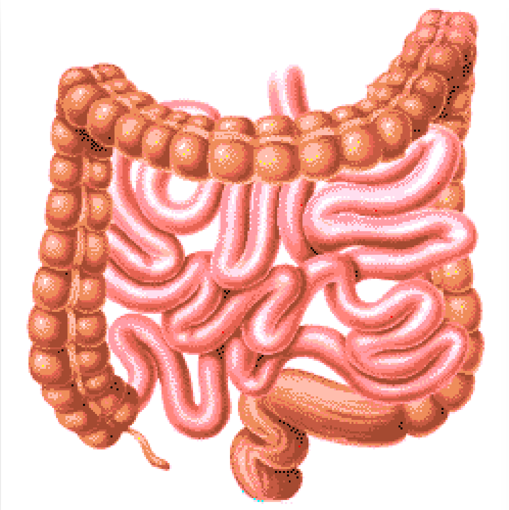

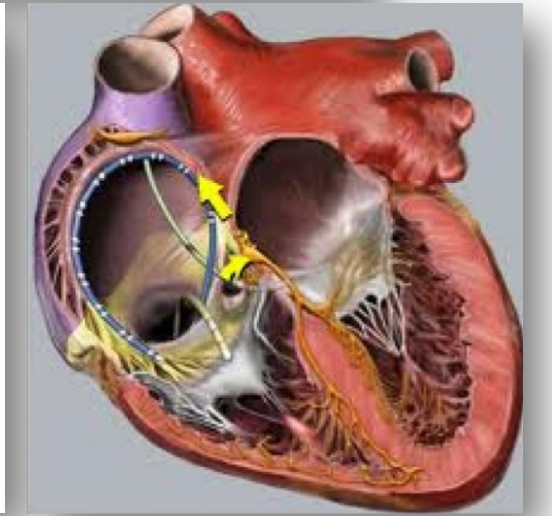

- **Equations governing physical phenomena** are well known
  - Linear and angular momentum balance
  - Mass balance
  - Energy balance
  - Thermodynamics principles…
- Modelling, based on weak or strong assumptions, typically involves
  - **geometry**, suggested by the particular shape of a body (structure: beam, plate, shell…)
  - **boundary conditions and interactions** with surrounding bodies
  - **material**, suggested by experimental tests on materials
- Modelling requires the **assessment of the correspondence with the real world** (validation).

Validation of Computational Mechanics Models

- **Equations governing physical phenomena** are well known
  - Linear and angular momentum balance
  - Mass balance
  - Energy balance
  - Thermodynamics principles…
- Modelling, based on weak or strong assumptions, typically involves
  - **geometry**, suggested by the particular shape of a body (structure: beam, plate, shell…)
  - **boundary conditions and interactions** with surrounding bodies
  - **material**, suggested by experimental tests on materials
- Modelling requires the **assessment of the correspondence with the real world** (validation).

Material Modelling

Material models can be roughly classified in

- **Phenomenological models**: Experimental behaviors are translated into mathematical equations governed by generic parameters, calibrated to best fit experimental data.
    1. Pros. Easy implementation, moderate computational cost.
    2. Contra. Unable to capture response under various loads for the same parameters.
- **Microstructural models**: The main characteristics of the microscopic organization of the material are explicitly included in the model.
    - Pros. Model parameters possess a direct physical meaning and remain the same for multiple loadings. The model is predictive.
    - Contra. Heavy implementation, high computational cost.

- **The nowadays challenge is on microstructural models (see metamaterials…)**

Fracking: inelastic hydro-mechanical coupling in geomechanics

- Fractures and discontinuities in natural rocks can evolve due to the action of gravity, superposed localized pressure, and shear tractions
- Fractures are related to porosity and permeability of rocks
- Actual great interest: damage induced by hydraulic stimulation in oil/gas reservoirs in view of increasing the reservoir production
- Resort to a multiscale Porous Brittle Damage Model [Pandolfi et al, JMPS, 2006]

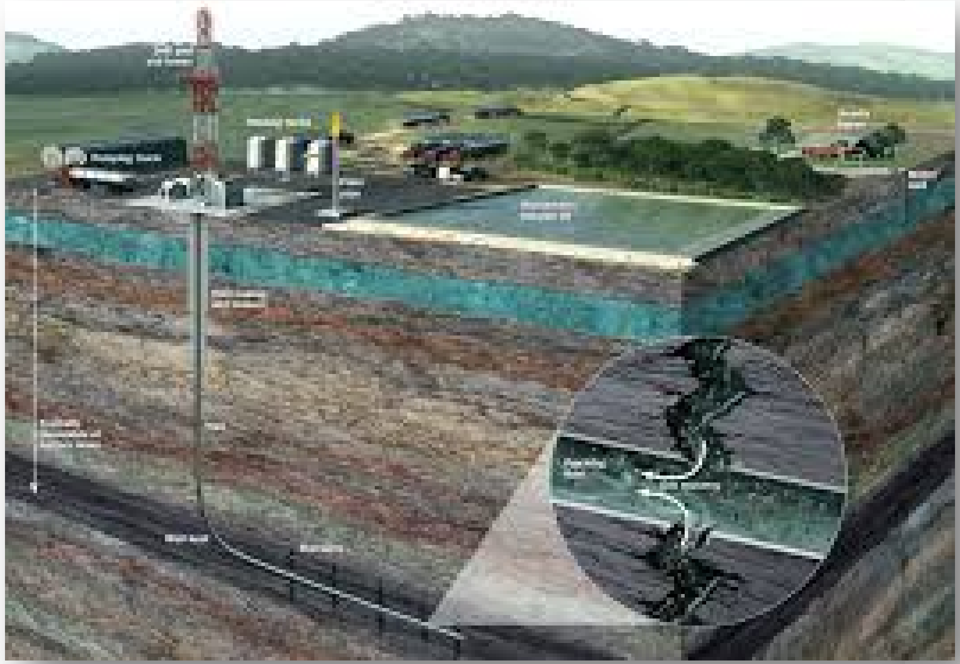

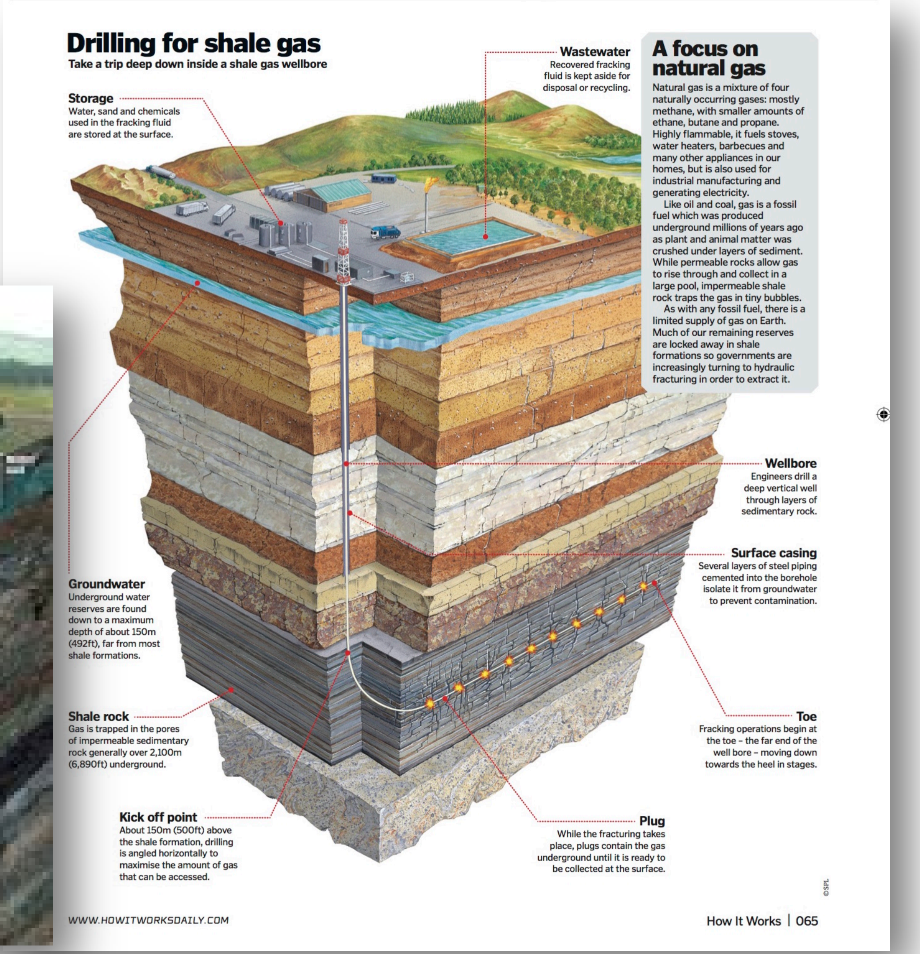

Kinematics of faults (linearized version, in total 6 mechanical parameters)

- Particular class of microstructures, consisting of nested families of equi-spaced cohesive faults bounding elastic (or any other) matrix material.
- Each family characterized by an orientation N and a spacing L (microstructural feature of the material that derives from optimality conditions on the system energy).
- The average macroscopic strain tensor admits the additive decomposition [De Bellis et al, EG, 2016]

$$\boldsymbol{\varepsilon} = \mathrm{sym}\nabla\boldsymbol{u} = \boldsymbol{\varepsilon}^{\mathrm{m}} + \boldsymbol{\varepsilon}^{\mathrm{f}}$$

$$\boldsymbol{\varepsilon}^{\mathrm{f}} = \mathrm{sym}\nabla\boldsymbol{u}^{\mathrm{f}} = \frac{1}{2L}(\boldsymbol{\Delta}\otimes\boldsymbol{N} + \boldsymbol{N}\otimes\boldsymbol{\Delta})$$

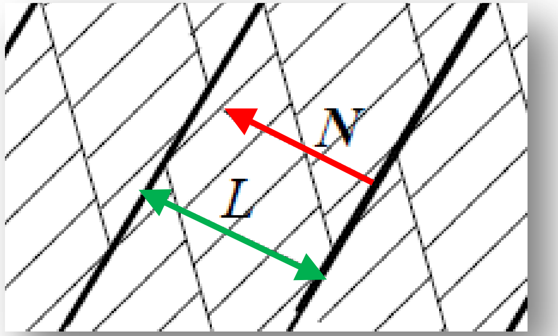

Displacement jump

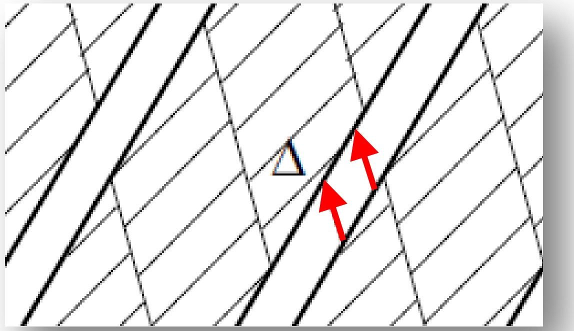

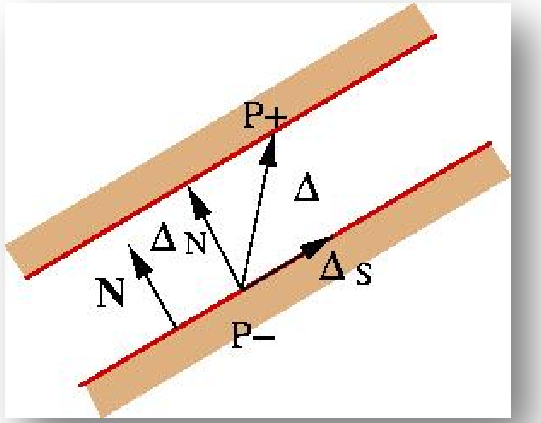

Variational characterization within time discretization

Hyperlastic matrix (E, ν)

$$W^{\mathrm{m}} = \frac{1}{2}\boldsymbol{\varepsilon}^{\mathrm{m}\,T} \cdot \boldsymbol{D}\boldsymbol{\varepsilon}^{\mathrm{m}}$$

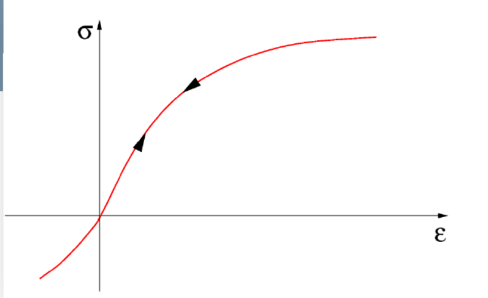

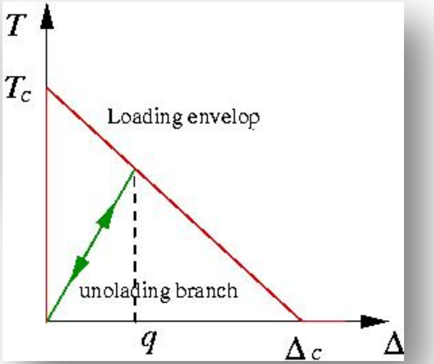

Cohesive micro-faults (G_c, T_c)

$$\Phi = \Phi(\Delta, \mathrm{q})\,, \qquad T = \frac{\partial \Phi(\Delta, \mathrm{q})}{\partial \Delta}$$

Frictional sliding (μ)

$$\psi^*(\dot{\boldsymbol{\Delta}}; \boldsymbol{\varepsilon}, \boldsymbol{\Delta}) = \mu \max\{0, \ -\boldsymbol{N} \cdot \boldsymbol{\sigma}\boldsymbol{N}\}\ |\dot{\boldsymbol{\Delta}}|$$

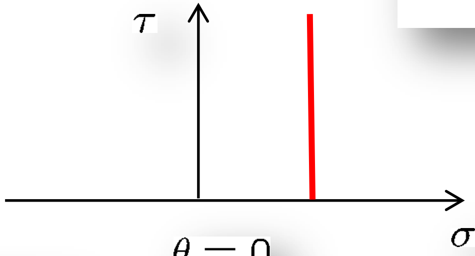

$\theta = 0$

Orientation (Rankine or Mohr-Coulomb) (T_c, μ)

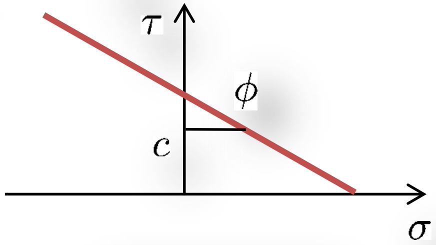

$\theta = \pi/4 - \phi/2$

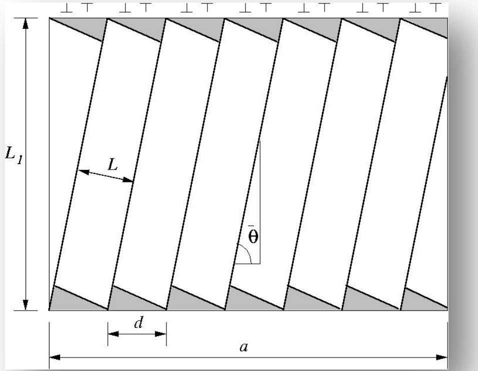

Spacing (L_0)

$$E^{\mathrm{mis}}(L_{n+1}) = \frac{C|\boldsymbol{\Delta}|^2}{L_n} \frac{1}{L_{n+1}} \log \frac{L_{n+1}}{L_0}$$

[De Bellis et al, EG, 2016]

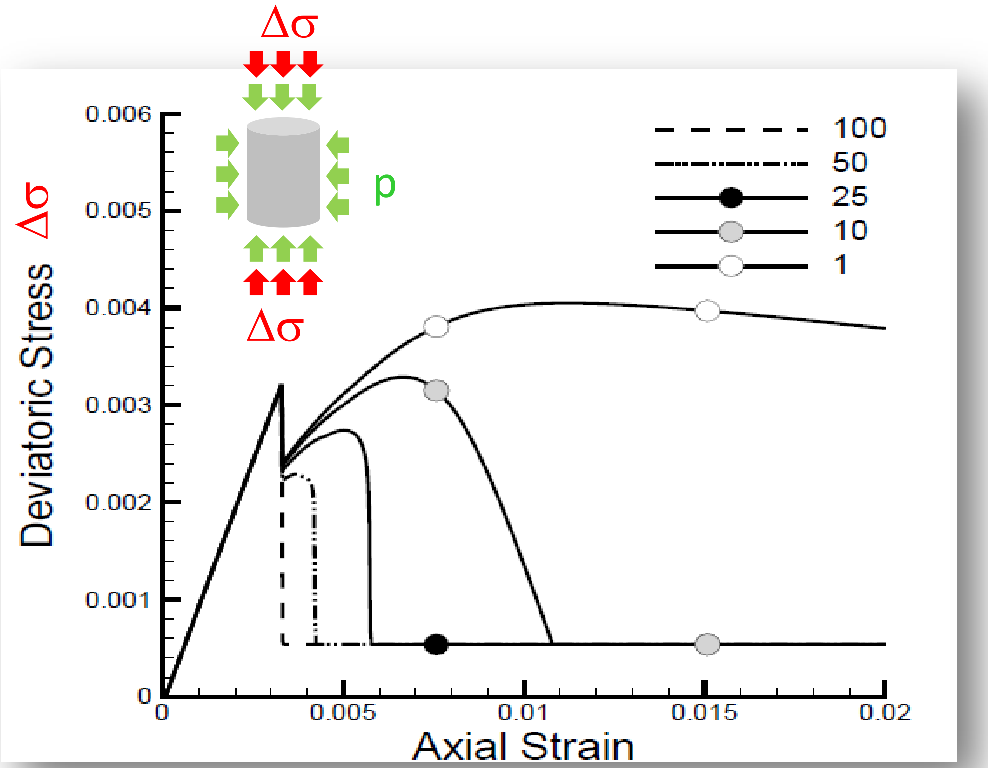

[De Bellis et al, EG, 2016]

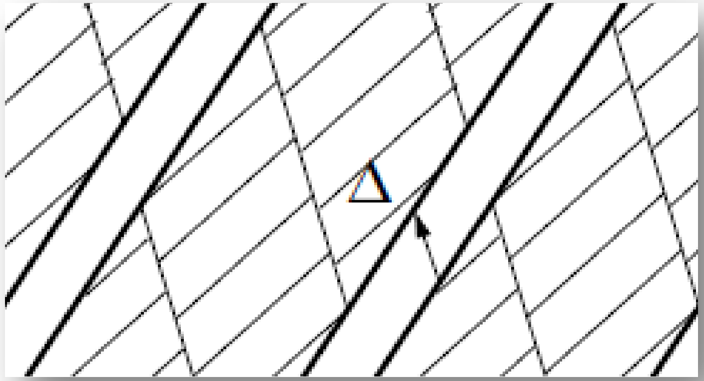

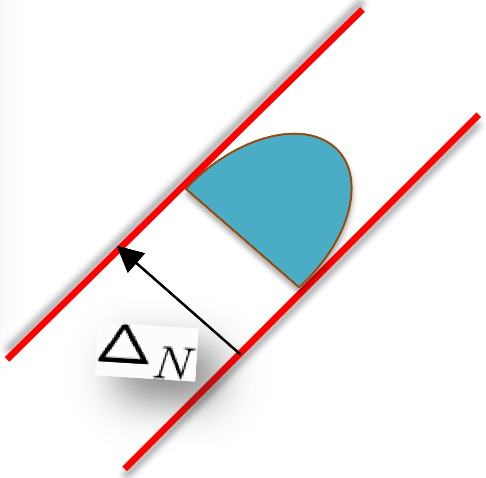

- Small L_0 : many distributed faults
- Large L_0 : a few localized faults

$$n = n^{\mathrm{m}} + n^{\mathrm{f}} = \varepsilon_v + \frac{\Delta_N}{L}$$

$$\kappa = \kappa^{\mathrm{m}} + \kappa^{\mathrm{f}} \ , \qquad \kappa^{\mathrm{f}} = \frac{1}{12} \frac{\Delta_N{}^3}{L} \left(\boldsymbol{I} - \boldsymbol{N} \otimes \boldsymbol{N} \right)$$

Interpretation of the global failure mechanism

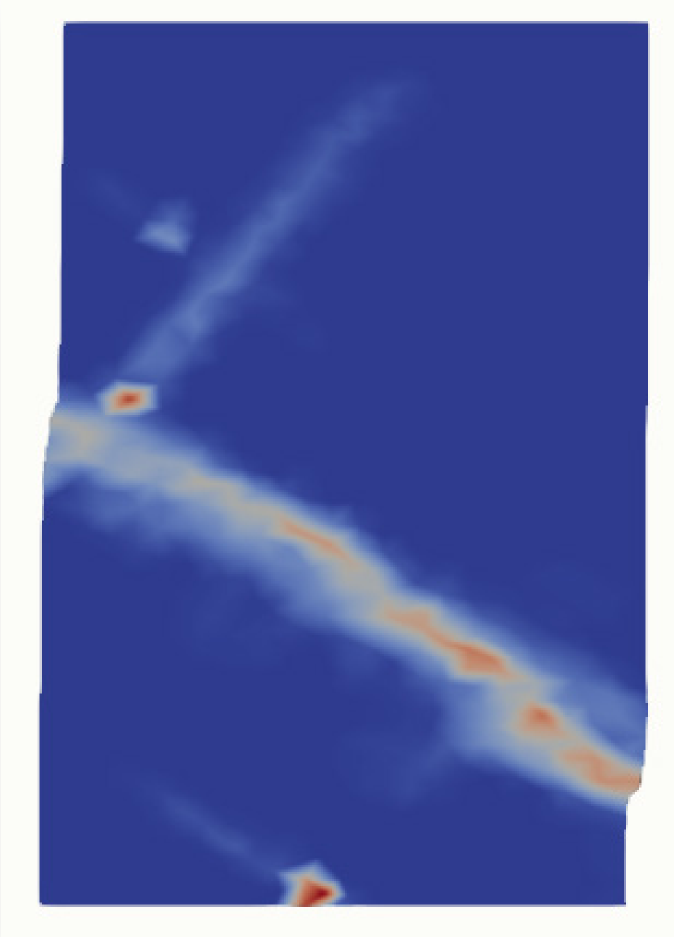

- The **global failure mechanism** derives from the **sliding within microstructures**.
- Microscopic cracks oriented almost orthogonally the macroscopic shear band.

Inside the damage

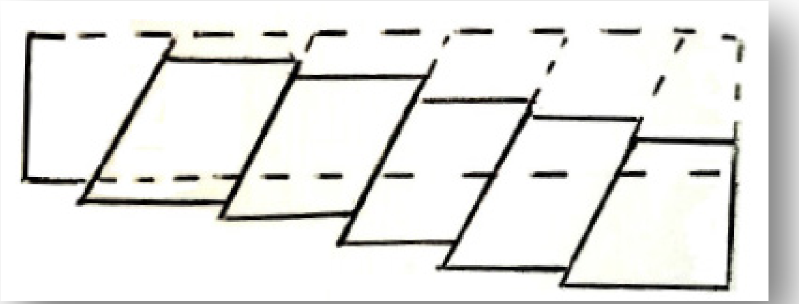

- No explicit modelling of fractures is requested by the approach.
- Macro-cracks are natural outcomes of the calculation defined by the distribution of the damaged zone.

Displacements NOT magnified

Hydro-mechanics porous media equations in linearized kinematics

- Linear momentum balance

$$\nabla \cdot \boldsymbol{\sigma} + \boldsymbol{b} = \mathbf{0}$$

- Continuity equation (fully saturated porous media, incompressible fluid and incompressible soil particles), *n* porosity, ε_v volumetric strain

$$\frac{\partial n}{\partial t} = -\nabla \cdot \boldsymbol{q} \qquad \frac{\partial n}{\partial t} = \frac{\partial \varepsilon_v}{\partial t}$$

- Terzaghi's effective stress principle, *p* pore pressure

$$\boldsymbol{\sigma} = \boldsymbol{\sigma}' + p\boldsymbol{I}$$

- Constitutive relations

$$\boldsymbol{\sigma}' = \boldsymbol{\sigma}'(\boldsymbol{\varepsilon})\,, \qquad \boldsymbol{\varepsilon} = \boldsymbol{\varepsilon}^{\mathrm{m}} + \boldsymbol{\varepsilon}^{\mathrm{f}}$$

- Constitutive relation for fluid flow in porous media (Darcy law), *h* hydraulic head, ***k*** permeability tensor

$$\mathbf{q} = -\boldsymbol{\kappa}\frac{\rho_f g}{\mu}\nabla h \qquad h = \frac{p}{\rho_f g} + z$$

Coupled field problem solution strategy

- Two field equation: linear momentum balance and continuity equation

$$\nabla \cdot \boldsymbol{\sigma} + \boldsymbol{b} = \mathbf{0}$$

$$\frac{\partial \varepsilon_v}{\partial t} = -\nabla \cdot \boldsymbol{q}$$

- Weak form (unknowns $\boldsymbol{u}$ and p, introduce the test functions v and η)

$$\int_V (\sigma'_{ij} + \delta_{ij} p) \frac{\partial v_j}{\partial x_i} dV = \int_{\Gamma_t} \bar{t}_j v_j d\Gamma + \int_V b_j v_j dV \, .$$

$$\int_V \frac{\partial n}{\partial t} \eta dV + \int_V \frac{\partial \eta}{\partial x_j} q_j dV = \int_{\Gamma_q} q_n \, \eta d\Gamma \, .$$

- After spatial discretization obtain the matrix form (similar to the consolidation equations)

$$\begin{cases} \boldsymbol{F}^{\text{ext}} - \boldsymbol{F}^{\text{int}}(\boldsymbol{U}) = \boldsymbol{H}^T \boldsymbol{P} \\ \\ \boldsymbol{K} \, \boldsymbol{P} = \boldsymbol{Q}^{\text{ext}} + \boldsymbol{H} \dot{\boldsymbol{U}} \end{cases}$$

- which is solved with a staggered approach (explicit in $\boldsymbol{u}$, implicit in p).

Material point: validation of the coupled behavior 1

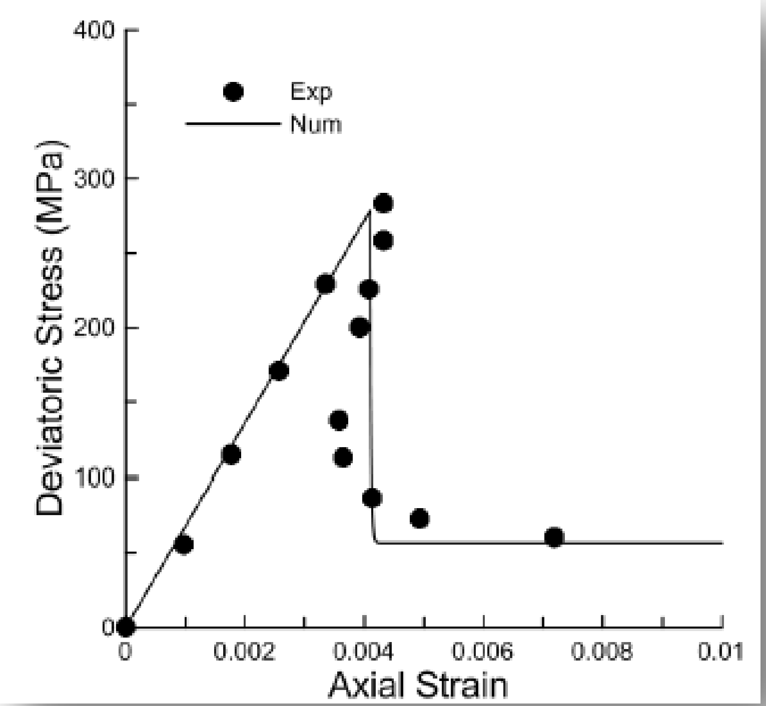

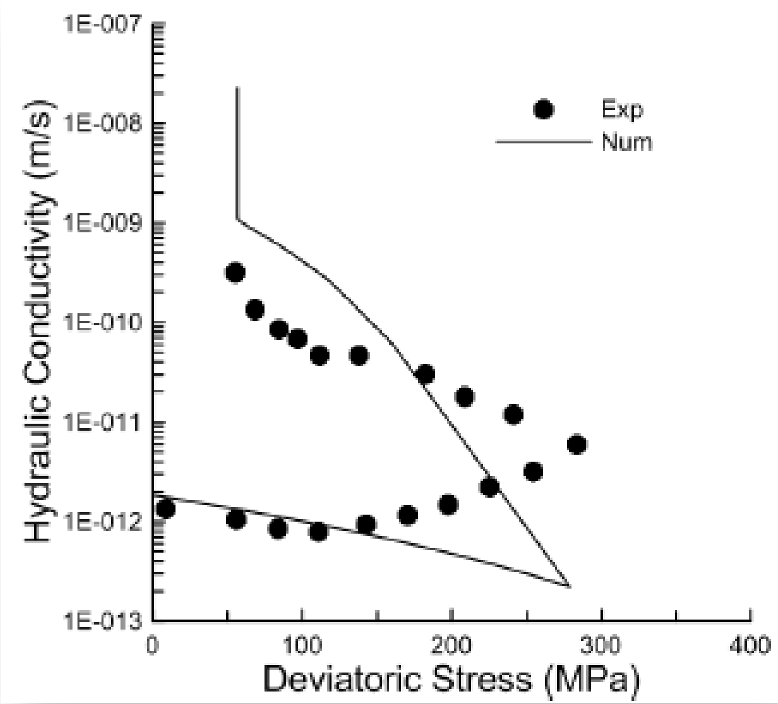

Inada sandstone (Kiyama et al, 1996)

Material point: validation of the coupled behavior 3

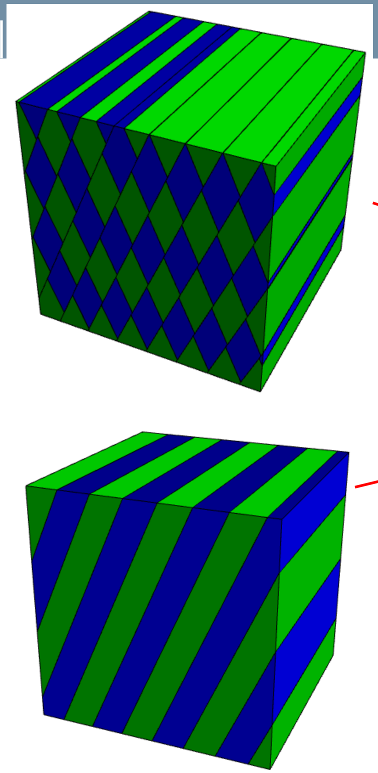

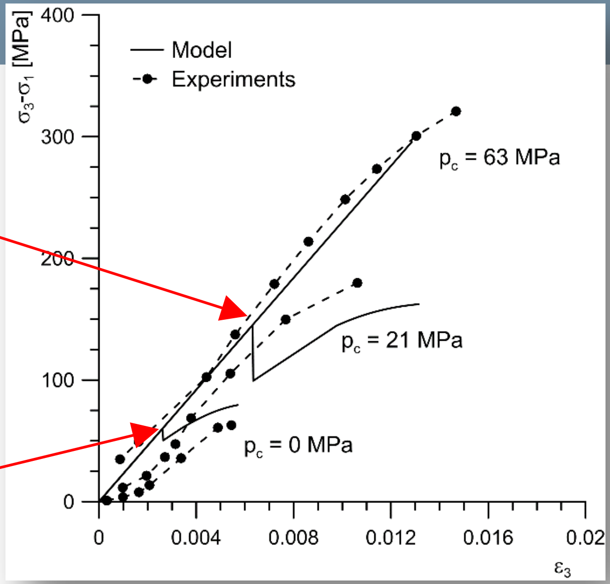

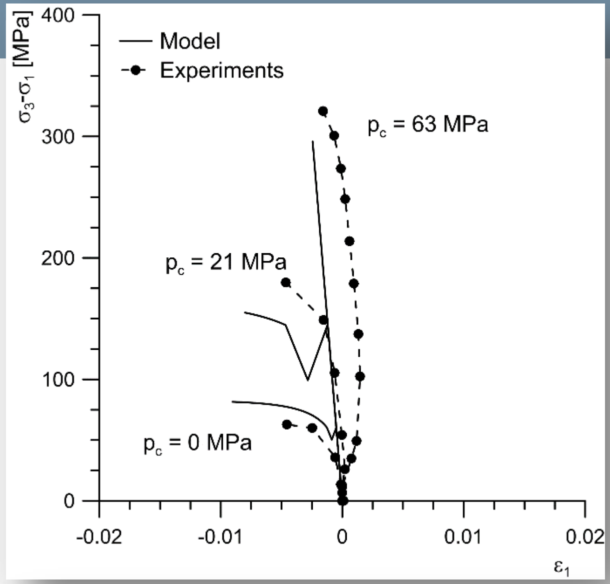

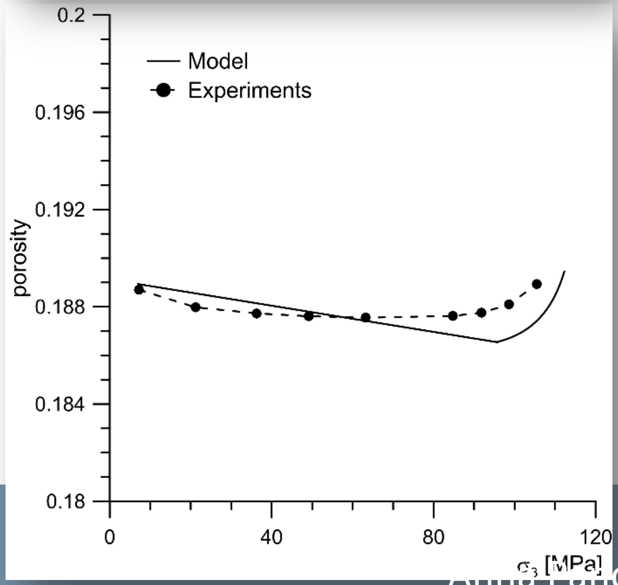

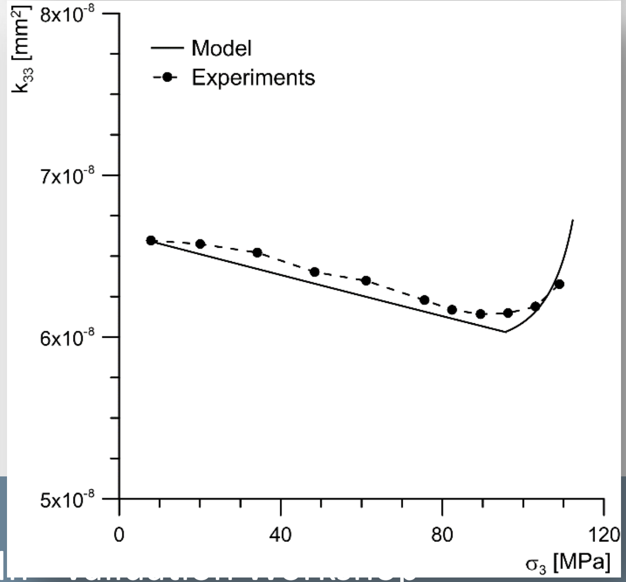

- Experiments on berea sandstone [Morita et al., 1992]
- Axial and radial stress strain curves
- Porosity and permeability in axial direction curves

[De Bellis et al, JMPS, 2017]

Boundary value problem 1. Dry compression of a block in plane strain

- Compressed block of sandstone with a stiff frame system applying plane strain boundary conditions [Yumlu & Ozbay, IJRMMS&G, 1995]
- Specimen size 30x30x10 mm
- Consider two confinement pressure

E [GPa]	28
ν	0.25
T_c[MPa]	83
G_c[N/mm]	100
ϕ [Deg]	52

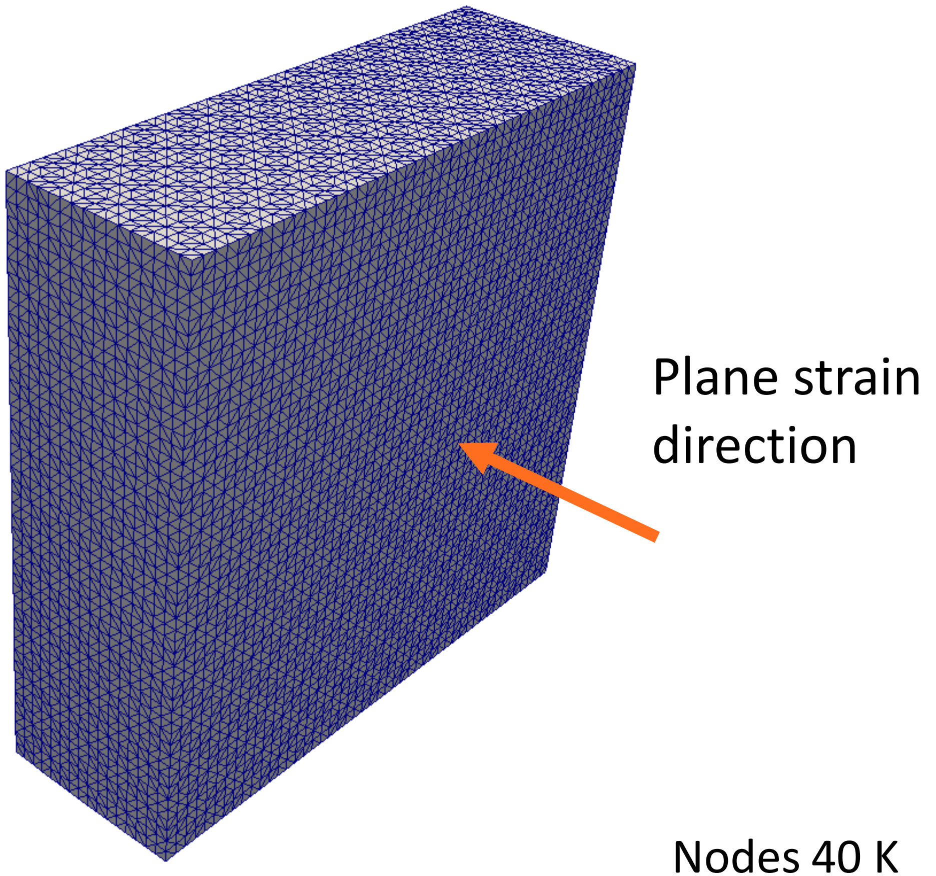

Nodes 40 K
10-node Tetrahedral Elements 30 K

Boundary value problem 1. Validation with global curves and failure pattern

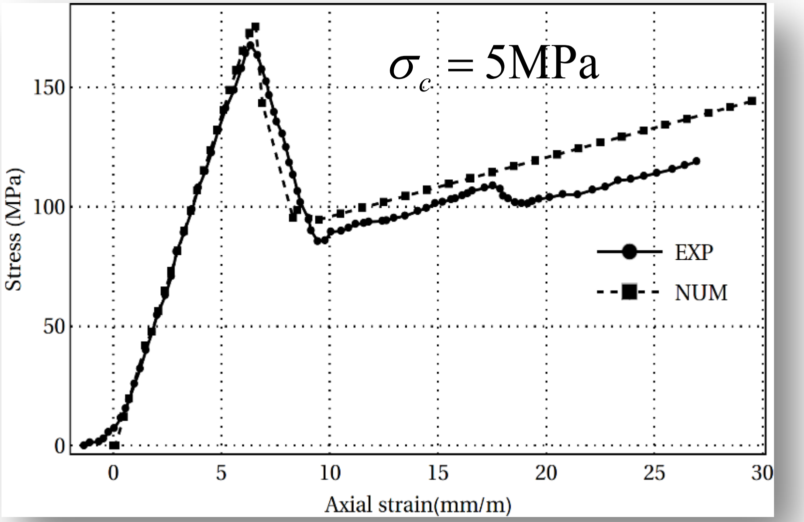

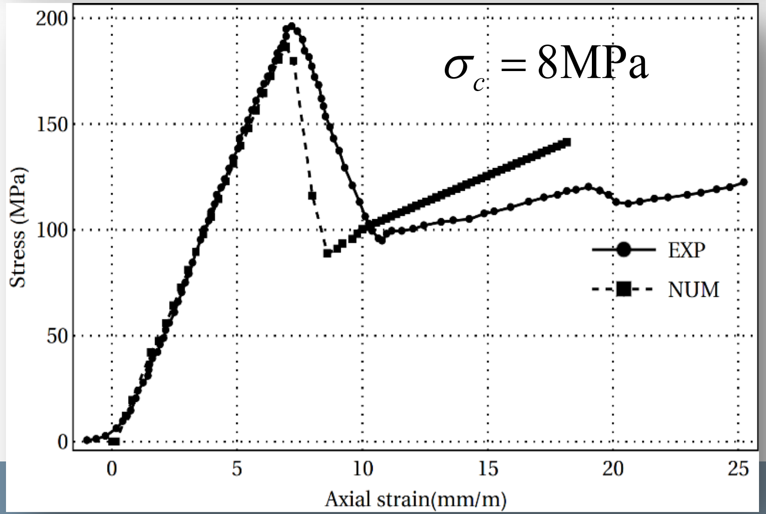

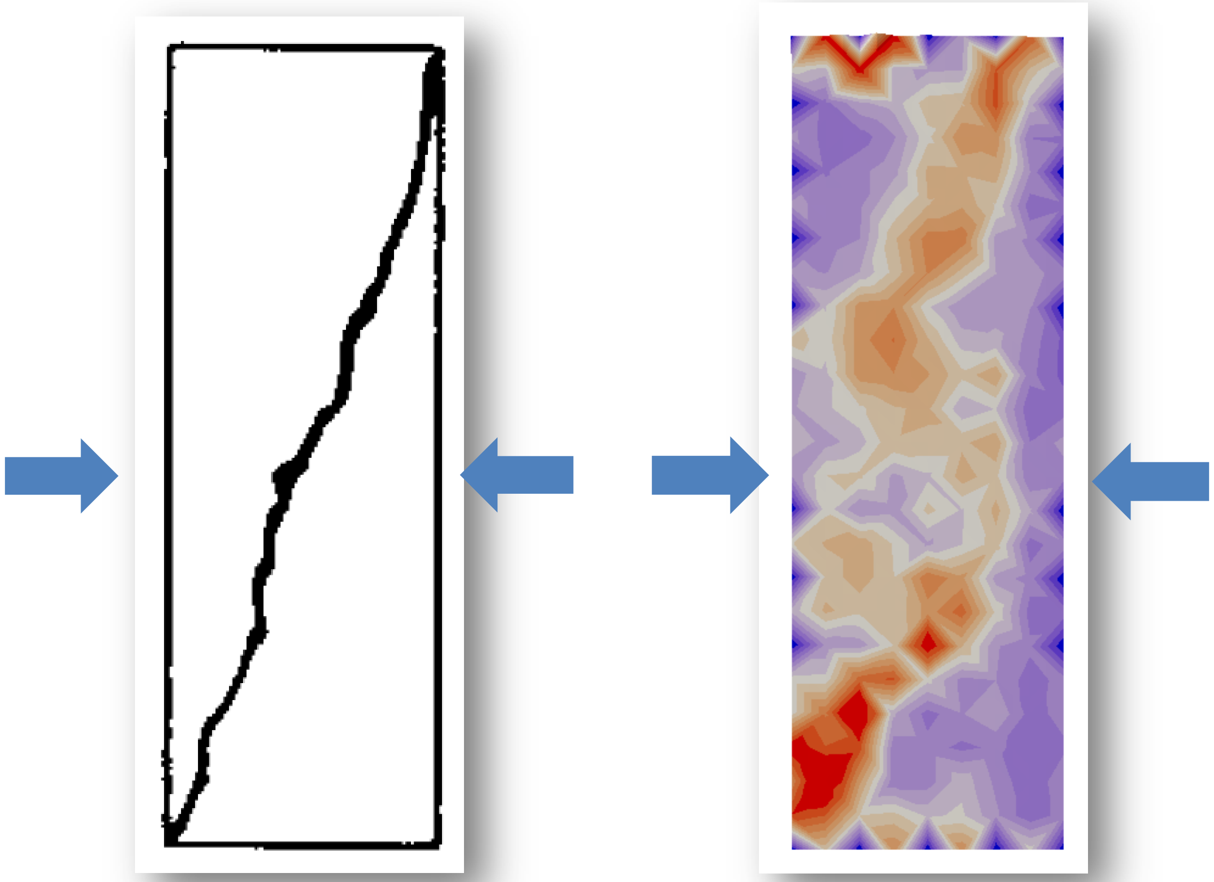

Experimental

Numerical

Boundary value problem 2. Triaxial loading of a cement block

Experimental data on a compressed block of cement pressurized with a fluid in a small cylindrical cavity at the center of the specimen [Athavale & Miskimins, SPE, 2008]

s_z = 24.2 MPa

s_x = 17.3 MPa

s_y = 10.4 MPa

Max fluid pressure = 20 MPa

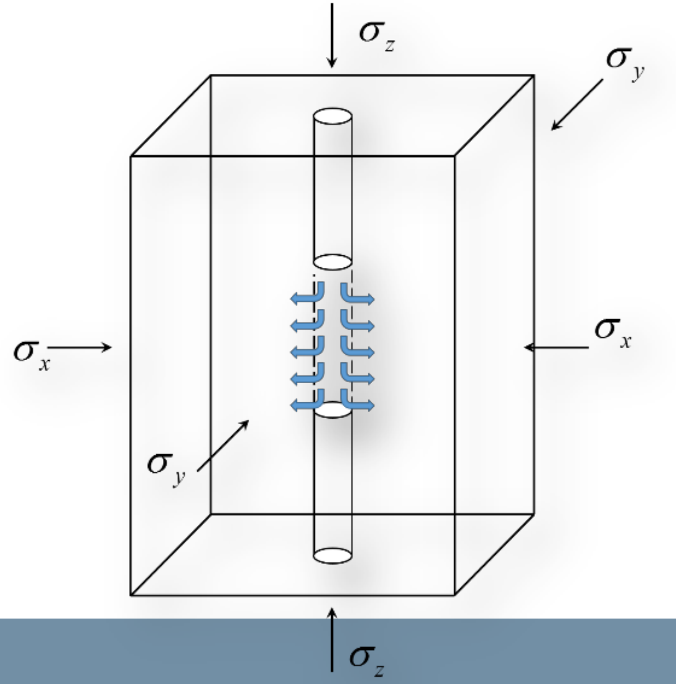

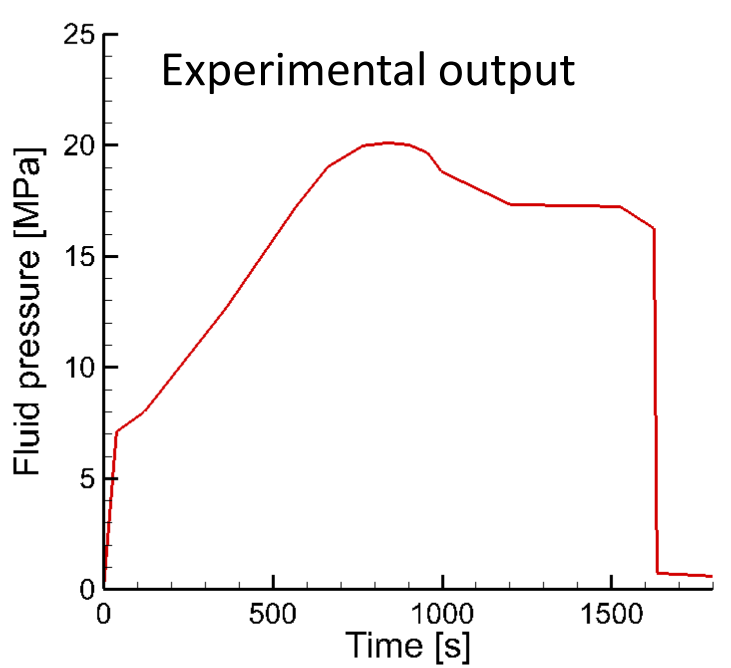

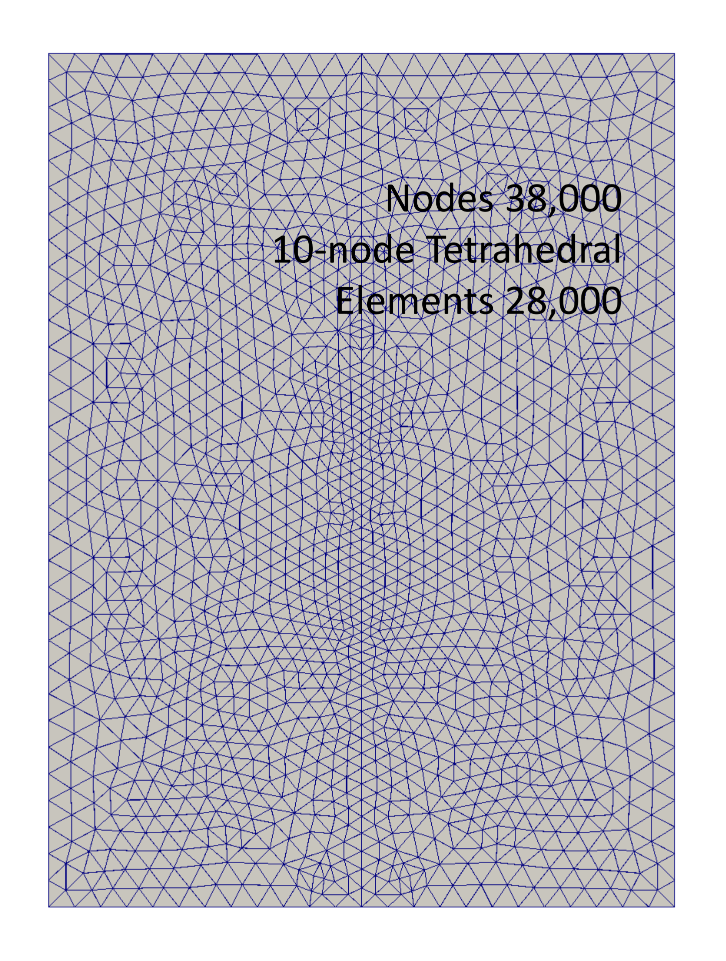

Boundary value problem 2. Validation with failure patterns

YZ plane (experiment)

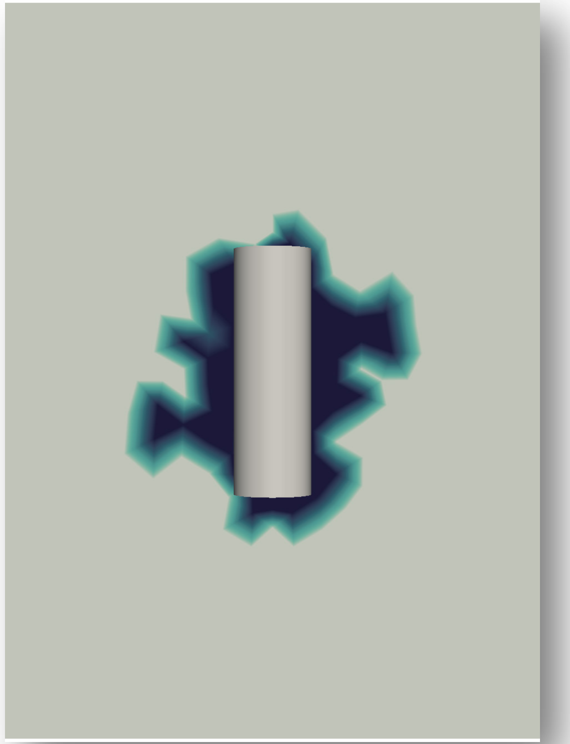

YZ plane (simulation)

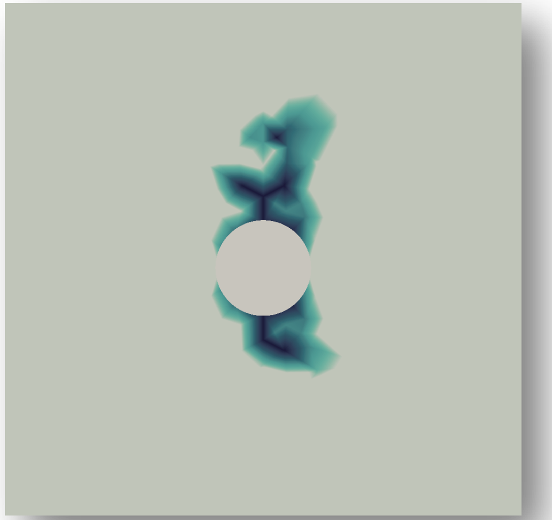

XY plane (simulation)

[De Bellis et al, JMPS, 2017]

- Missing strength properties estimated from the literature. Assume G_c = 100 N/m, T_c = 5 MPa, and ϕ = 31 degrees. A posteriori damage variable (0 no damage, 1 full damage)

Boundary value problem 2. Validation with global curves

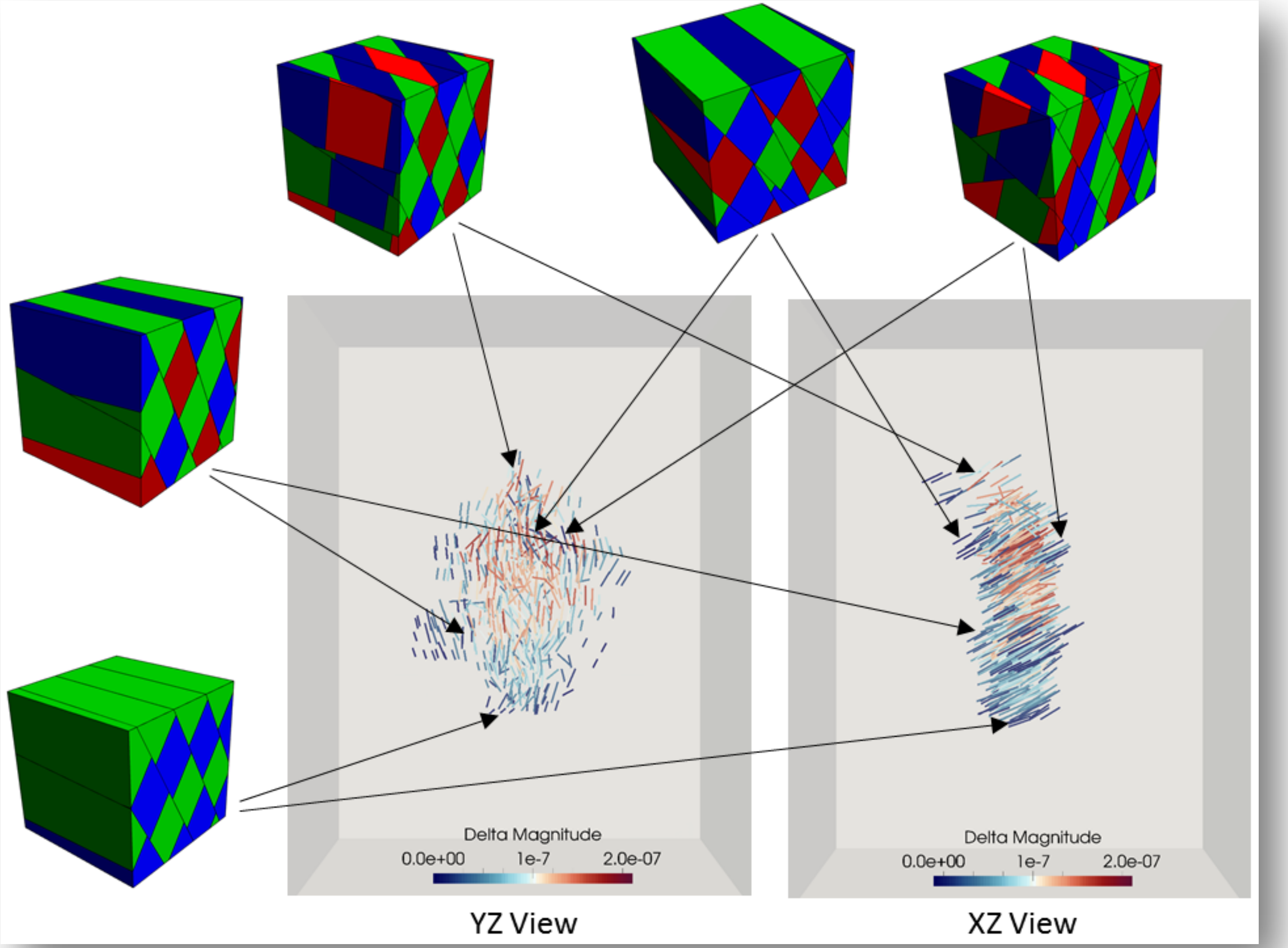

- Faults form according the Mohr–Coulomb criterion.
- Colored lines: aligned along the fault normal, colored as the magnitude of the sliding jump.

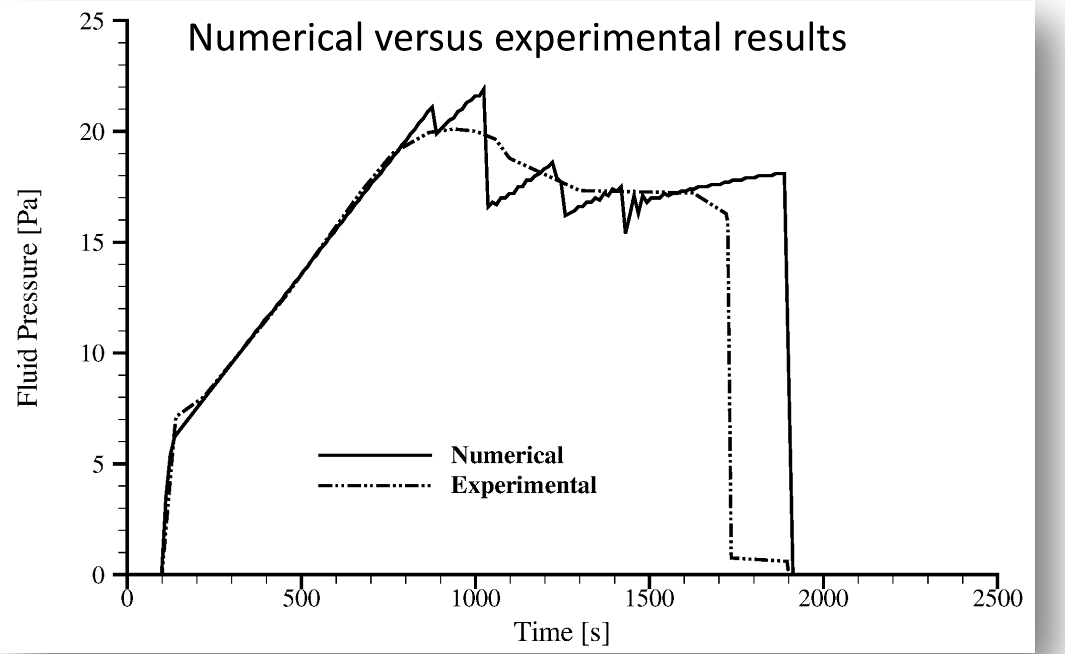

Boundary value problem. A simulation of a fracking process

- Most material and geometry data are unknowns
- Only the relevant feature of the fracking process are described
- The elementary fracking unit is the cluster. Requested
  - Orientation
  - Diameter D
  - Spacing L
  - Cluster length h ≤ L

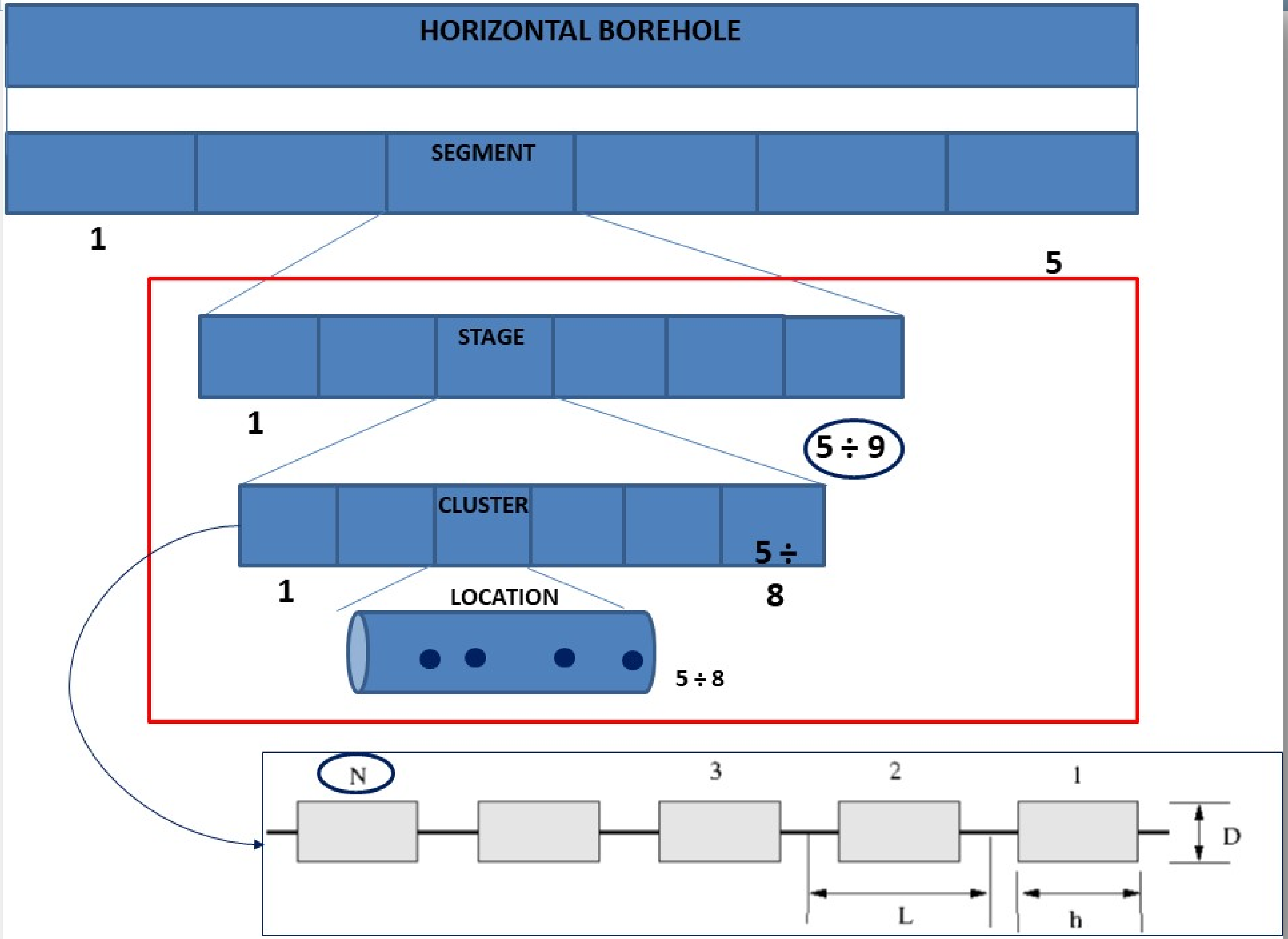

Example of a 10 cluster fracking process in a horizontal well

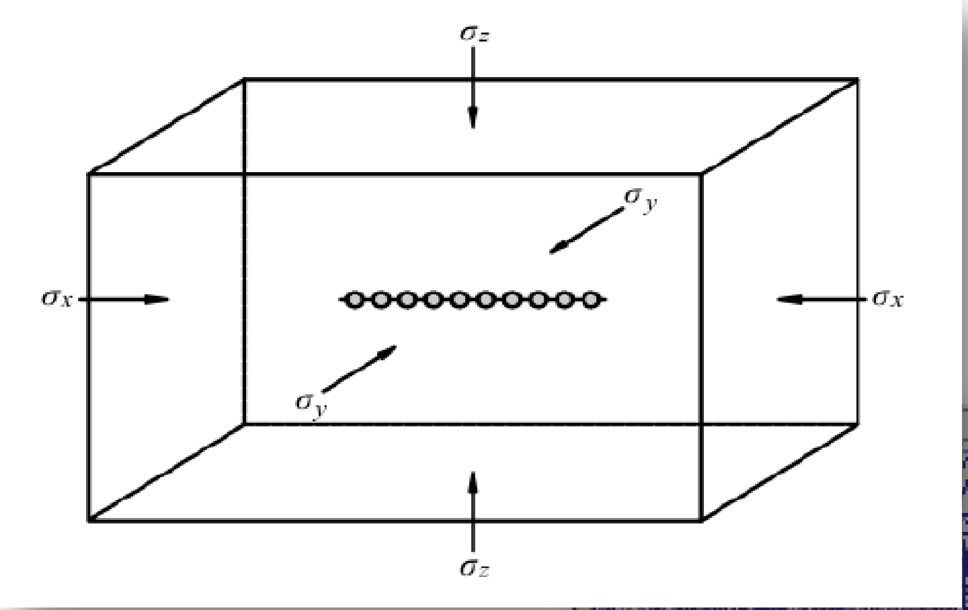

Reservoir size: 3.5 x 2.5 x 2.5 km

Adopted finite element discretization in the central zone where the injections take place

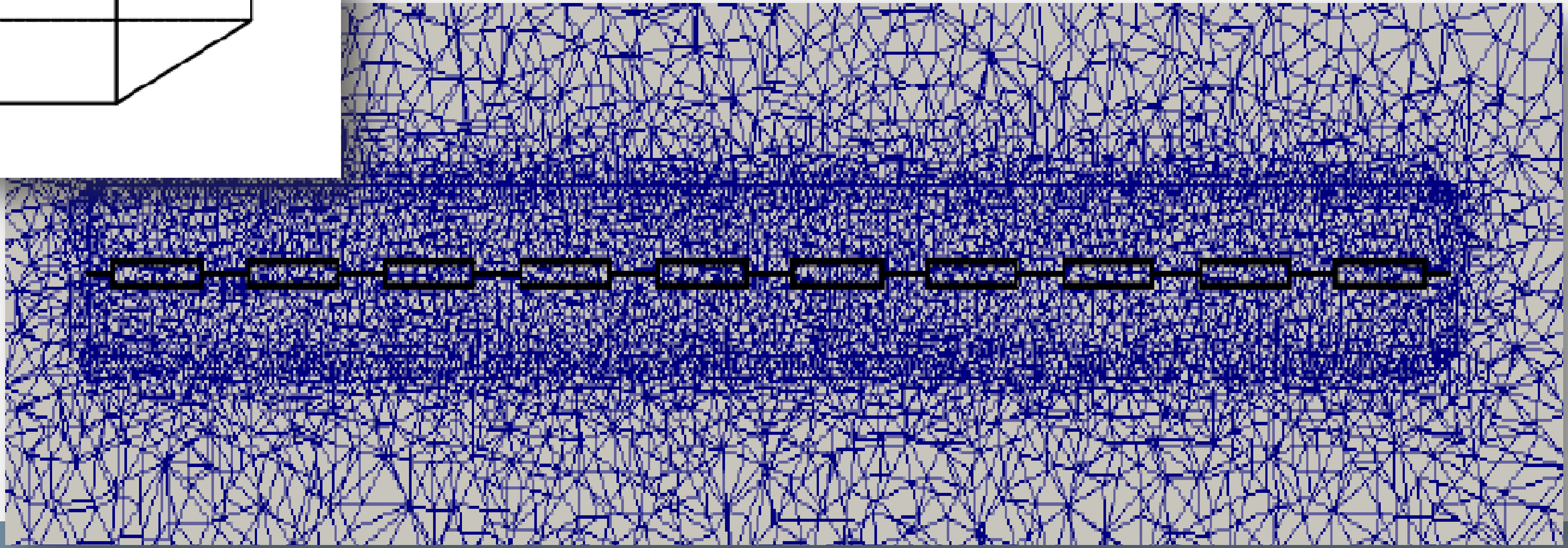

Simulation results: fracture volume and fracture surface

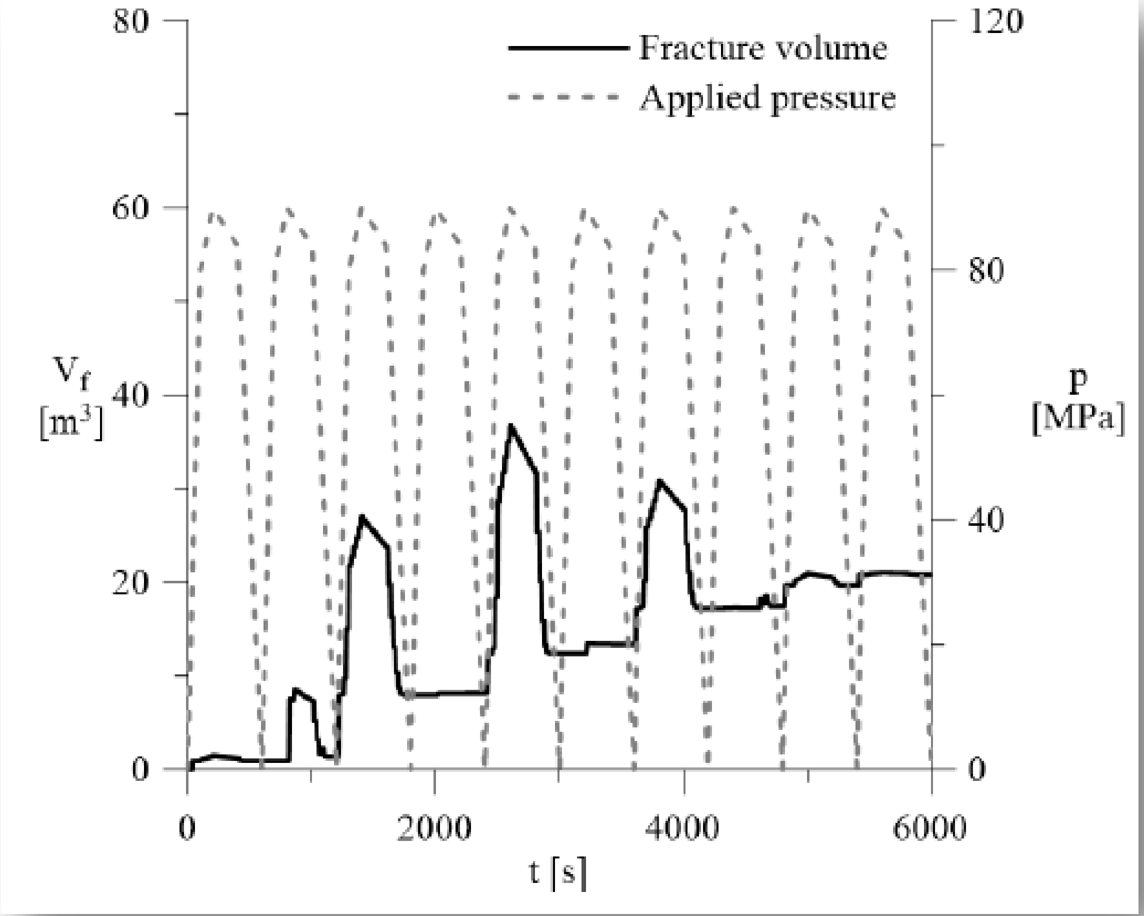

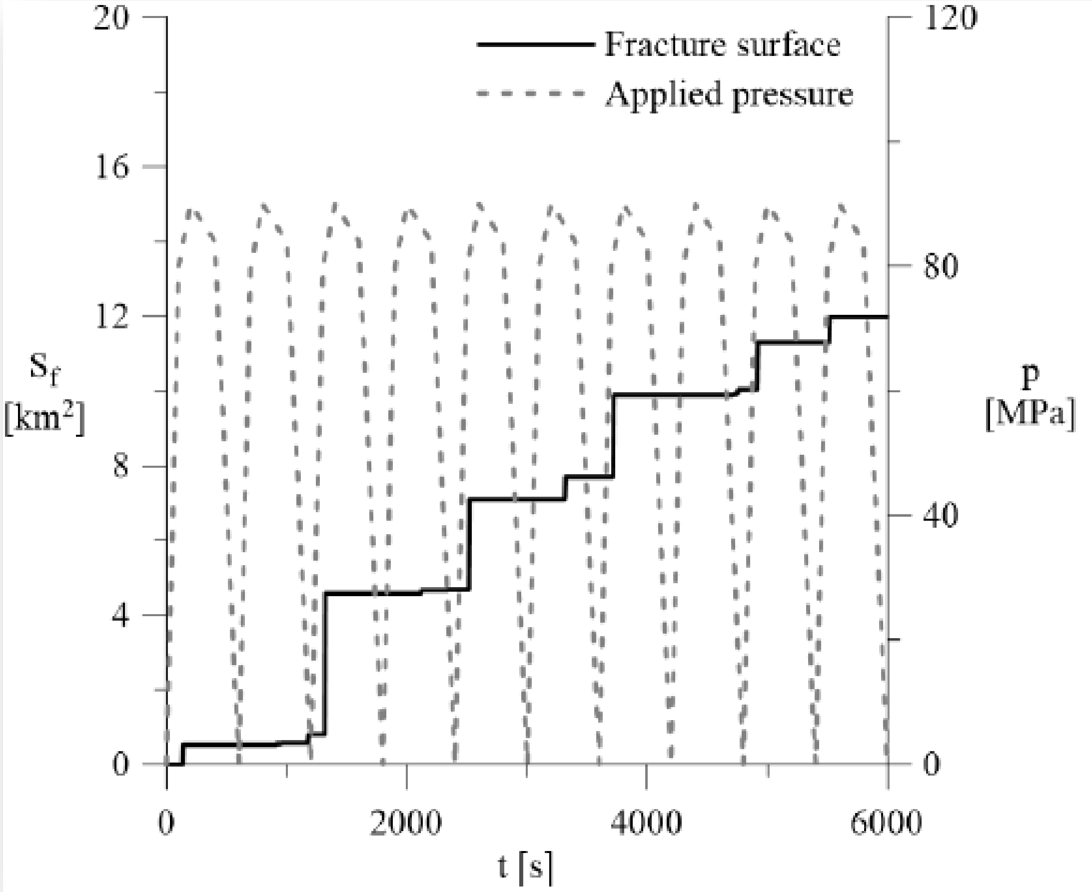

Fracture volume history and fracture surface history, together with the applied fluid pressure

Permeability change after 10 fracked clusters

Longitudinal effective stress after 10 fracked clusters

Active (deformable under an electric stimulus) bio-tissues

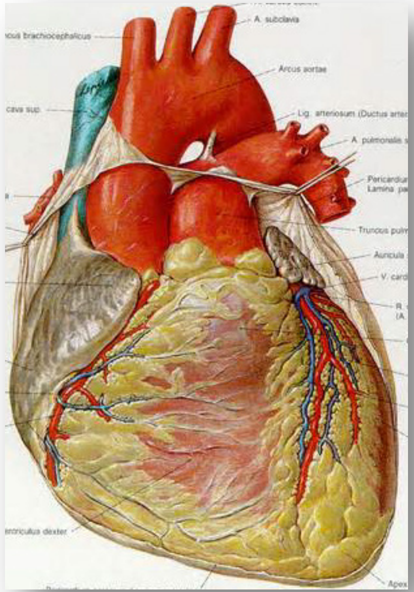

Heart

Muscles

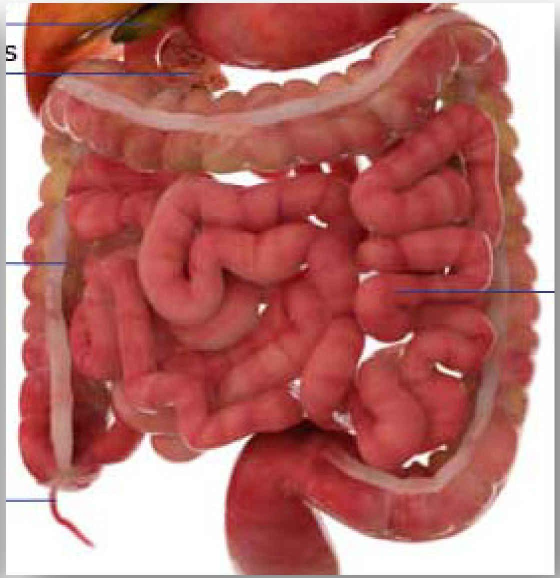

Intestines

Eye's iris

- Biological active tissues: heart, skeletal muscle, gastro-intestine, eye's iris…
- Show the ability to develop contractions, producing the mechanical forces necessary to the organ's function.
- Contractions originated by an electric potential due to transmembrane (K^-, Na^-) and intracellular currents (Ca^{++})

Anisotropy associated to spatial dispersion of collagen fibers

Pulmonary aortic valve (PAV)

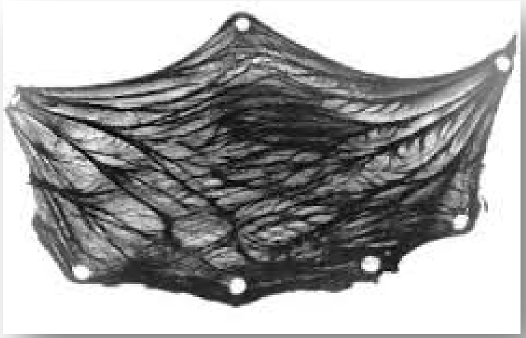

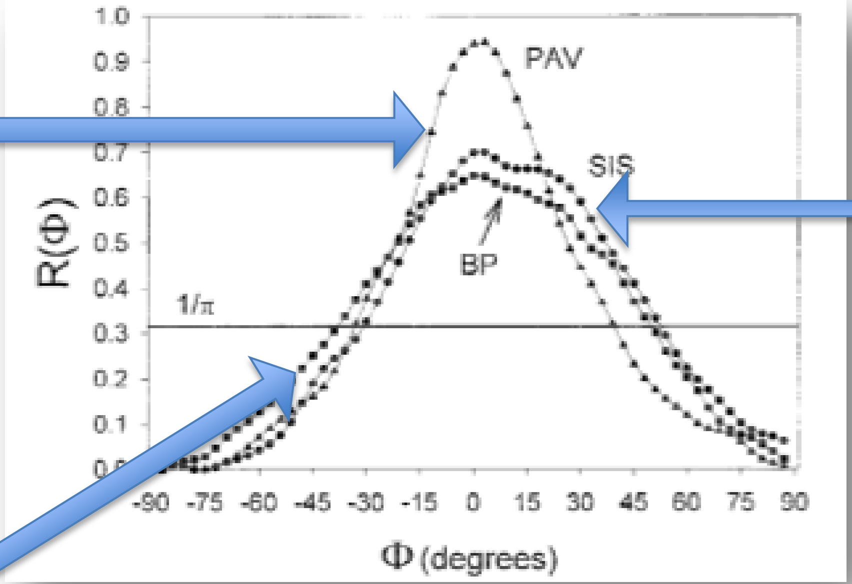

Small intestine submucosa (SIS)

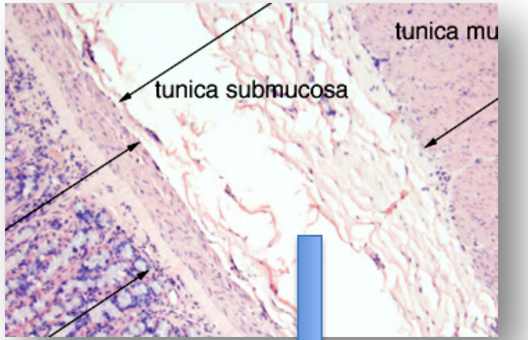

[Sacks et al. 1999]

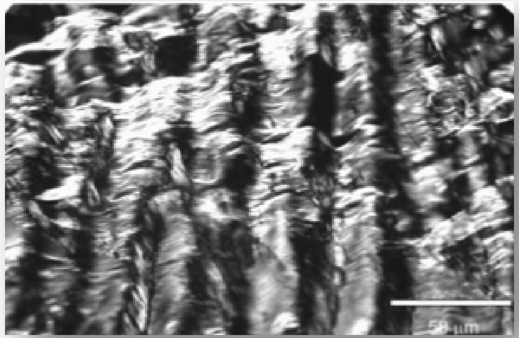

Bovine pericardium (BP)
(photomicroscopy, optical analysis)

- Fiber reinforced tissues
- Dispersed fibers with statistical properties
- Presence of two distinct populations of fibers

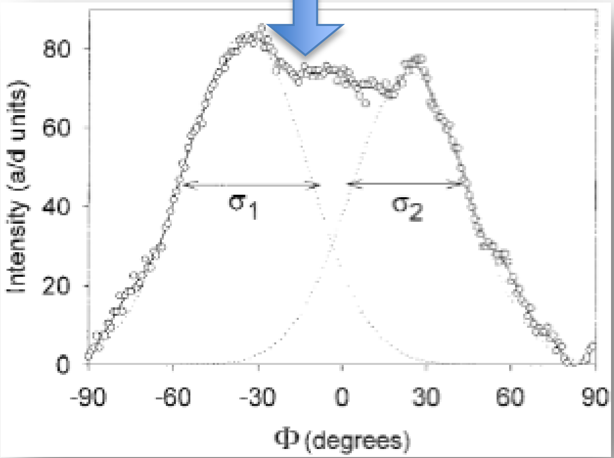

Mechanical passive behavior of muscles: anisotropy, hysteresis, viscosity

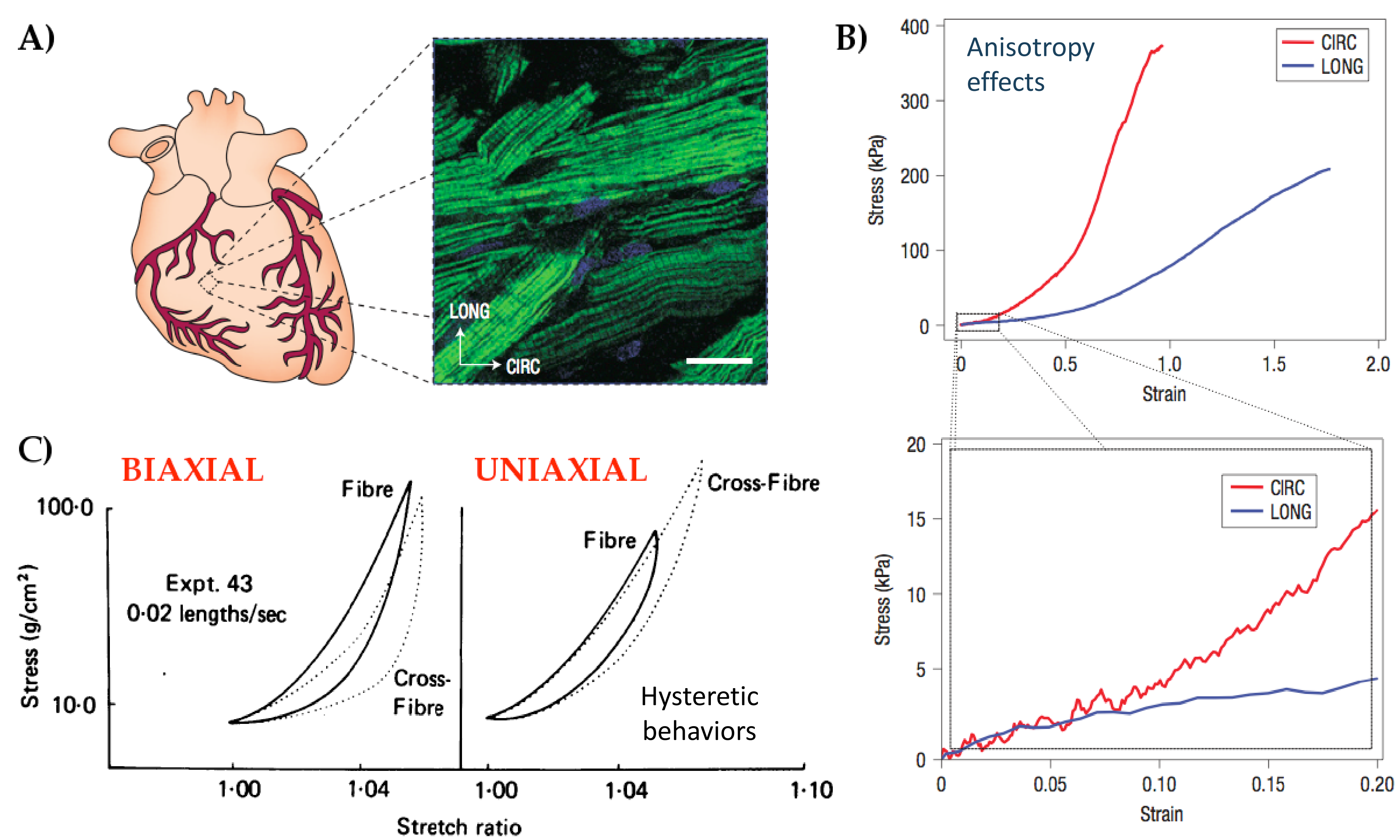

Engelmayr et al 2008

Distributed fibers: healthy to diseased

- Spatial distribution of muscular fibers at the mesoscopic level
- In healthy physiological condition, observe small dispersion of fibers following a Gaussian profile
- In some pathological cases observe large and less regular dispersion
- Fiber dispersion characterize both the response of the material in both passive and active behaviors

Erikkson et al, 2013

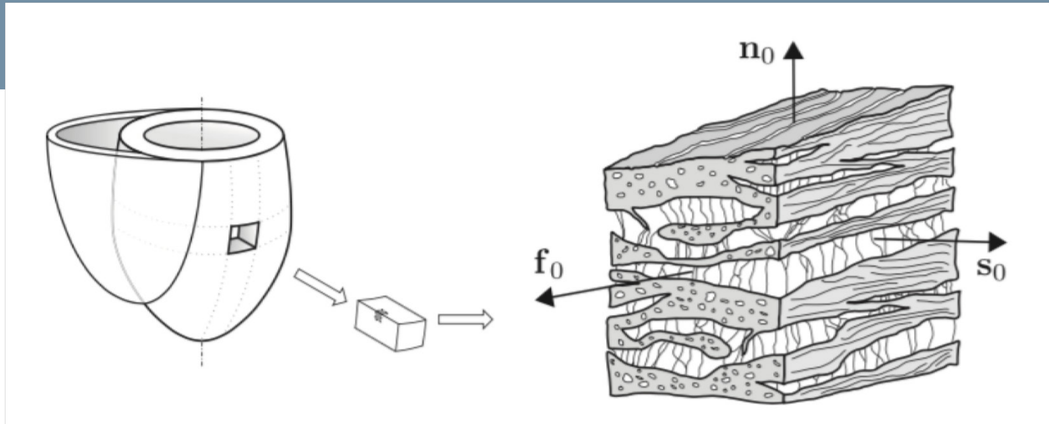

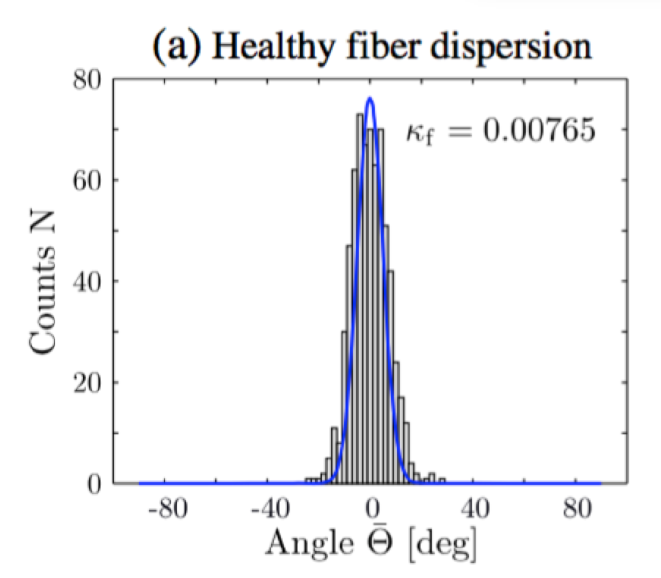

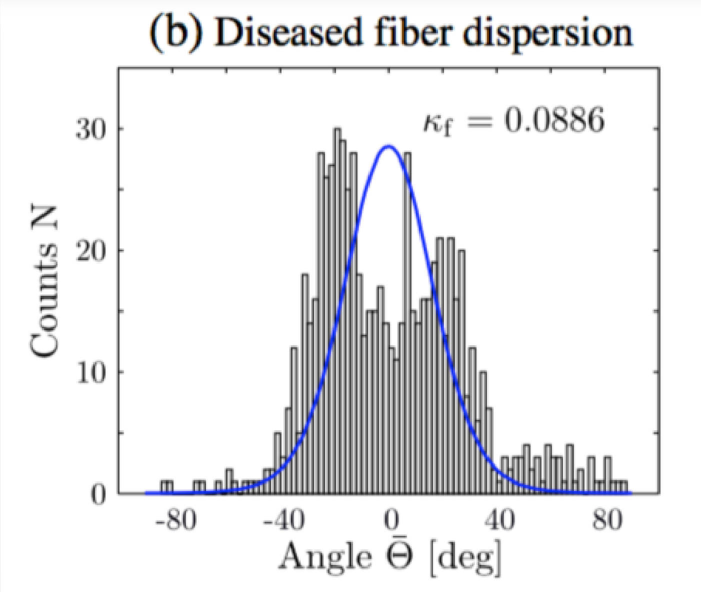

Active behavior: simplified FitzHugh-Nagumo model of excitation

- Prototype of an exciting dynamic system. Based on two variables:
- A *voltage-like variable* φ having cubic nonlinearity that allows regenerative self-excitation via a fast feedback
- A *recovery variable w* having a linear dynamics that provides a slower negative feedback.
- The cell membrane consists of three components:
  - capacitor C_m representing the membrane capacitance;
  - nonlinear current-voltage device for the fast current *i*,
  - resistor g_L, inductor and battery E_L in series for the recovery current *w*.
- Governing equations:

$$\frac{\partial \varphi}{\partial t} = F(\varphi) - i - w, \qquad \frac{\partial w}{\partial t} = a(bw - c\varphi)$$

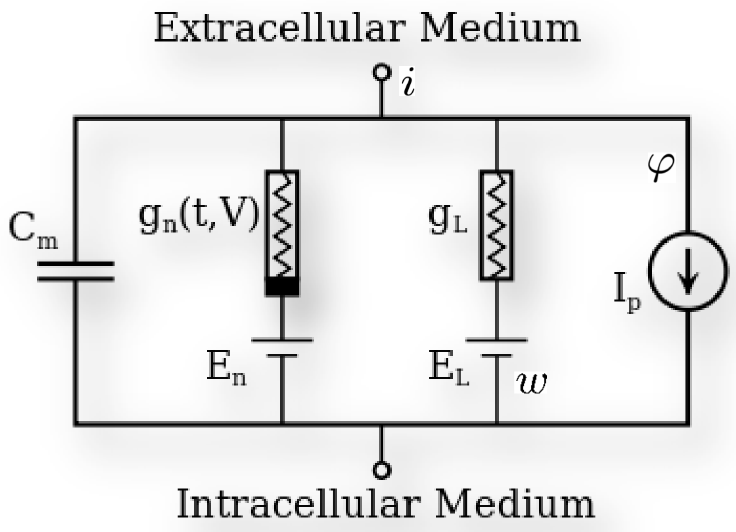

Electro-mechanics balance equations in finite kinematics

- Linear and angular momentum balance: $\mathbf{V}$ velocity, $\mathbf{P}$ first Piola-Kirchhoff stress tensor, $\mathbf{F}$ deformation gradient, ρ_0 material density (plus corresponding b.c.):

$$\rho_0 \frac{d\mathbf{V}}{dt} = \nabla_{\mathbf{X}} \cdot \mathbf{P} + \rho_0 \mathbf{B}, \qquad \mathbf{P}\mathbf{F}^T = \mathbf{F}\mathbf{P}^T$$

- Energy balance: U internal energy, **D** dielectric displacement or induction, φ electric potential, **E** electric field:

$$\dot{U} = \mathbf{P} : \dot{\mathbf{F}} + \mathbf{E} \cdot \dot{\mathbf{D}}, \qquad \mathbf{E} = -\nabla_{\mathbf{X}} \varphi$$

- Electric potential dynamics through the cell membrane described by a diffusion-reaction equation, combined with intercellular coupling in cardiac tissue. $\mathbf{Q}$ is the conductivity tensor [Rogers & McCulloch, 1994; Aliev & Panfilov, 1996]:

$$C_m \frac{d\varphi}{dt} = \frac{1}{J} \nabla_{\mathbf{X}} \cdot (\mathbf{Q} \nabla_{\mathbf{X}} \varphi) - k\varphi(\varphi - a)(\varphi - 1) - w\varphi + I_{\mathrm{ext}}$$

- Recovery current circulation equation (L inductance, R resistance, φ_0 potential gain):

$$L \frac{\partial w}{\partial t} + Rw = \varphi - \varphi_0$$

Finite kinematics approach

- Active deformation can be easily introduced in the mechanical framework under the assumptions of
- Multiplicative decomposition of the deformation gradient:

$$\mathbf{F} = \mathbf{F}^e \mathbf{F}^a, \qquad \mathbf{F} = \frac{d\mathbf{x}}{d\mathbf{X}},$$

- The free energy density decomposes in elastic and inelastic parts with separation of the arguments

$$A(\mathbf{F}, \mathbf{E}) = A^e(\mathbf{F}^e) + A^a(\mathbf{F}, \mathbf{E})$$

- Frame indifference considerations imply dependence on $\mathbf{C} = \mathbf{F}^{\mathrm{T}}\mathbf{F}$

$$A(\mathbf{C}, \mathbf{E}) = A^e(\mathbf{C}^e) + A^a(\mathbf{C}, \mathbf{E})$$

- Constitutive laws

$$\mathbf{P}^E = \partial_{\mathbf{F}} A(\mathbf{C}, \mathbf{E}), \qquad \mathbf{D} = \partial_{\mathbf{E}} A(\mathbf{C}, \mathbf{E})$$

The inelastic (active) part accounts for the deformation of the tissue due to the electric field.

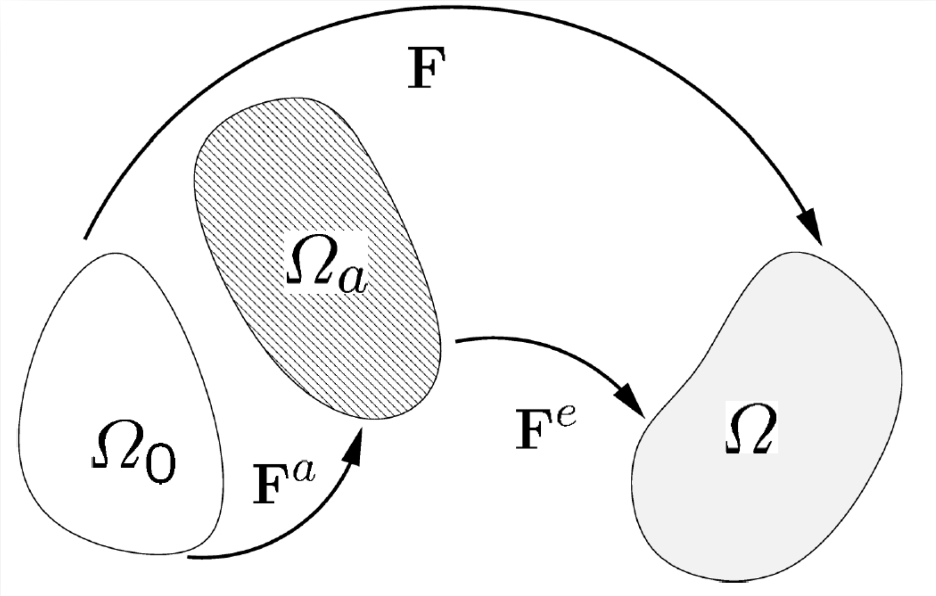

Lagrangian formulation **[Dorfmann & Ogden, 2006; Cherubini et al, 2008; Rosato & Miehe, 2010; Ask et al, 2010, 2012, 2013]**

Constitutive modeling: active stress versus active strain

- Active stress: usual approach in cardiac electro-mechanics (McGarry et al 2010)
- Active strain: described by means of eigen-deformations (Ambrosi et al 2011)
- A definition of active stress consistent with active strain can be derived through thermodynamics arguments that allow for the definition of all the constitutive relationships (Gizzi et al, 2015):

$$\mathbf{P} = \partial_{\mathbf{F}} A^e(\mathbf{C}^e) + \partial_{\mathbf{F}} A^a(\mathbf{C}, \mathbf{E}) = \mathbf{P}^p + \mathbf{P}^a$$

- Advantages:
  - The general structure of the constitutive equations will be extended easily to any mechanical behavior, accounting for viscosity, damage, anisotropy, growth;
  - Other coupled phenomena, such as electro-chemical diffusion, are easily accounted for (Yang et al, 2006)

- Convenient expression of elastic strain energy density for fibrous tissues through **C**'s invariants (**a** is a preferential fiber orientation an $\mathbf{A} = \mathbf{a} \otimes \mathbf{a}$) to model the passive behavior:

$$A^e(\mathbf{C}^e, \mathbf{A}) = A^e_{\text{vol}}(J^e) + A^e_{\text{iso}}(\bar{I}_1, \bar{I}_2) + A^e_{\text{aniso}}(\bar{I}_4) \qquad \overline{C}^e = J^{e-2/3}\mathbf{C}^e \qquad I_4 = \overline{\mathbf{C}}^e : \mathbf{A}$$

- Probability density function of the orientation, with normalization and symmetry properties

$$\int_\omega \bar{\rho}(\mathbf{a}) d\omega = \int_o^\pi \int_0^{2\pi} \bar{\rho}(\mathbf{a}) \sin\theta d\phi d\theta = 4\pi\,,\ \bar{\rho}(-\mathbf{a}) = \bar{\rho}(\mathbf{a})$$

- Amount of fibers in the range $\bar{\rho}(\mathbf{a}) \sin\theta d\phi d\theta$

$$[(\theta, \theta + d\theta), (\phi, \phi + d\phi)]$$

- Average of a function $f(\mathbf{a})$ over the unit sphere is

$$< f >= \int_\omega \bar{\rho}(\mathbf{a}) f(\mathbf{a})\, d\omega$$

- Expression of the single fiber strain energy density

$$A_{\text{aniso}}(I_4) = \frac{k_1}{2k_2} \exp[k_2(I_4 - 1)^2] - \frac{k_1}{2k_2} \qquad I_4 = \mathbf{C} : \mathbf{a} \otimes \mathbf{a}$$

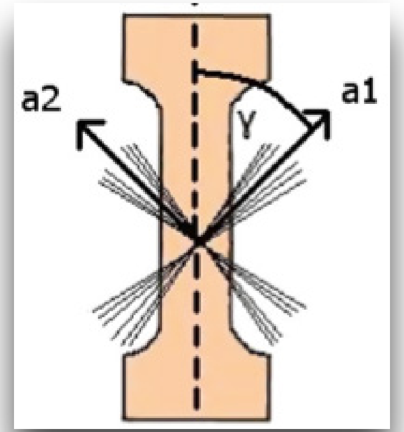

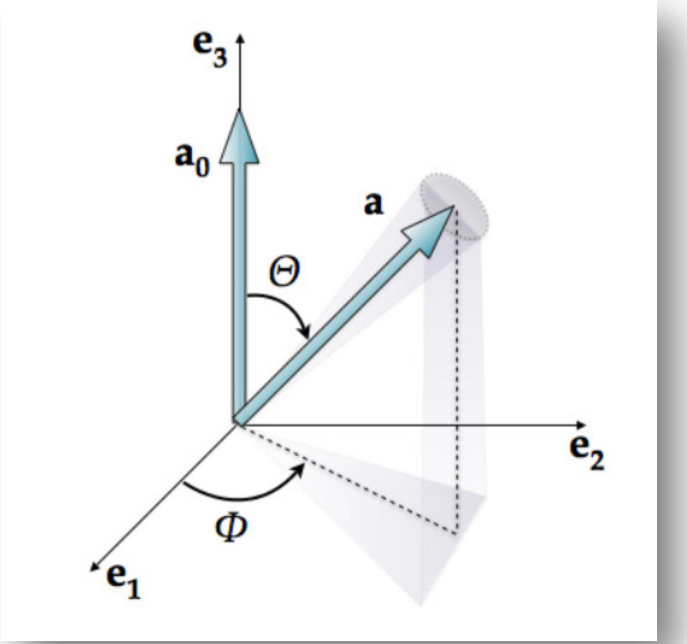

Passive behavior: approximations of distributed fiber models

- Anisotropic strain energy of the fiber distribution

$$< A_{\text{aniso}} >= \int_{\omega} \bar{\rho}(\mathbf{a}) A_{\text{aniso}}(I_4)\, d\omega$$

- Closed forma approximations of the energy allows for the analytical derivation of stress and elasticity tensors. Among others:
- Generalized structure tensor model (GST) [**Gasser et al, 2006**]

$$A^{GST}_{\text{aniso}} \approx A_{\text{aniso}}(I_4^*) \qquad I_4^* = I_4^*(\mathbf{H}) =< I_4 > \qquad \mathbf{H} =< \mathbf{A} >$$

- Variance model (V) **[P & Vasta, 2012]**

$$A^{V}_{\text{aniso}} \approx A_{\text{aniso}}(I_4^*)(1+K^*\sigma^2_{I_4}) \qquad \sigma^2_{I_4} = \sigma^2_{I_4}(\mathbf{H}, \mathbb{H})$$

$$\mathbb{A} = \mathbf{A}\otimes\mathbf{A} = \mathbf{a}\otimes\mathbf{a}\otimes\mathbf{a}\otimes\mathbf{a}\,, \qquad \mathbb{H} =< \mathbb{A} >= \int_{\omega} \mathbb{A}\rho(\mathbf{a}) d\omega$$

- The models have been studied for von Mises distributions.
  - Both models show a good performance for fibers with strongly aligned orientations
  - V model performs better for more dispersed sets of fibers

Verification of the approximated material models with analytical results

Assume a von Mises type distribution, characterized by a unique dispersion coefficient b. Compare approximations with exact integration **[P. & Vasta 2012]**

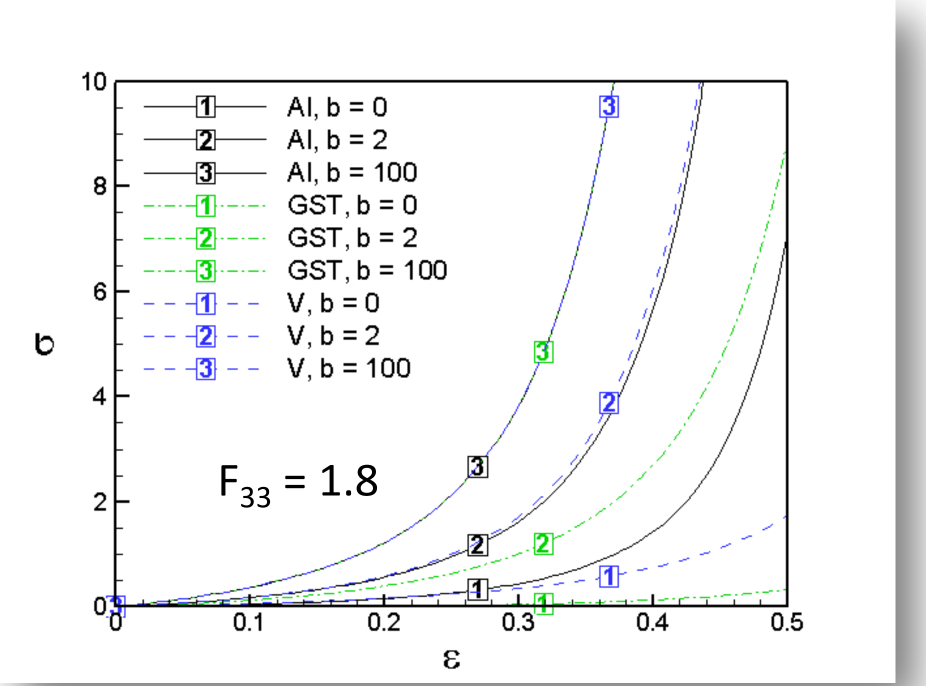

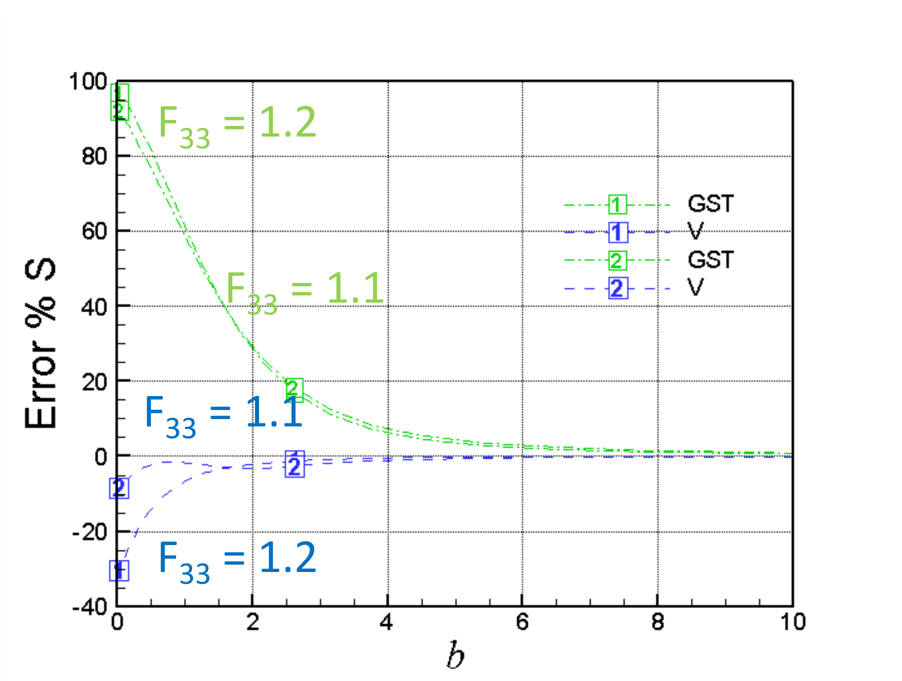

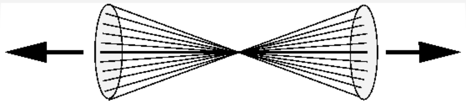

$$E = \frac{S_{33}^{AI} - S_{33}}{S_{33}^{AI}} \times 100$$

Ansatz: active behavior of distributed fiber models

- Extend the statistical treatment to active behavior. The generic orientation $\boxed{\mathbf{a}}$ (and thus the tensor $\boxed{\mathbf{A}}$) is an aleatoric variable, thus both elastic and inelastic energy depend are aleatoric

$$A(\mathbf{C},\mathbf{E},\boxed{\mathbf{A}}) = A^e(\mathbf{C}^e,\boxed{I_4}) + A^a(\mathbf{C},\mathbf{E},\boxed{\mathbf{A}})$$

- Want to generalize the inelastic free energy adopted for a deterministic orientation [**Gizzi et al, 2015**]

$$A^a(\mathbf{C},\mathbf{E},\mathbf{A}) = -\frac{1}{2}\varepsilon_0 J\mathbf{E}\left[\mathbf{C}^{-1} + \chi(\mathbf{C}(\mathbf{E}),\mathbf{A})\right]\mathbf{E}$$

- And assume an additive decomposition of the permittivity tensor

$$\chi(\mathbf{C}(\mathbf{E}),\boxed{\mathbf{A}}) = \chi_{\text{iso}}\left(J(\mathbf{E})\right) + \chi_{\text{aniso}}\left(I_4(\mathbf{E},\boxed{\mathbf{A}})\right)$$

- We begin by defining the active deformation gradient $\mathbf{F}^a$, making that strong assumption that the active mapping excludes rigid rotations and leads only to proper deformations (length and angle changes).

[Pandolfi et al, 2016]

Kinematics of the active deformation

- Assume the following expression for the directional deformation gradient (single fiber):

$$\mathbf{F}^a(\mathbf{a}) = g_1(\mathbf{E}) + g_2(\mathbf{E}, \boxed{\mathbf{a}})\,\boxed{\mathbf{A}} = \mathbf{F}^{aT}$$

$$g_1(\mathbf{E}) = f_1(\mathbf{E})\,, \quad g_2(\mathbf{E},\mathbf{a}) = f_2(\mathbf{E}) \cos \boxed{\beta}, \quad \cos \boxed{\beta} = \mathbf{m} \cdot \boxed{\mathbf{a}}$$

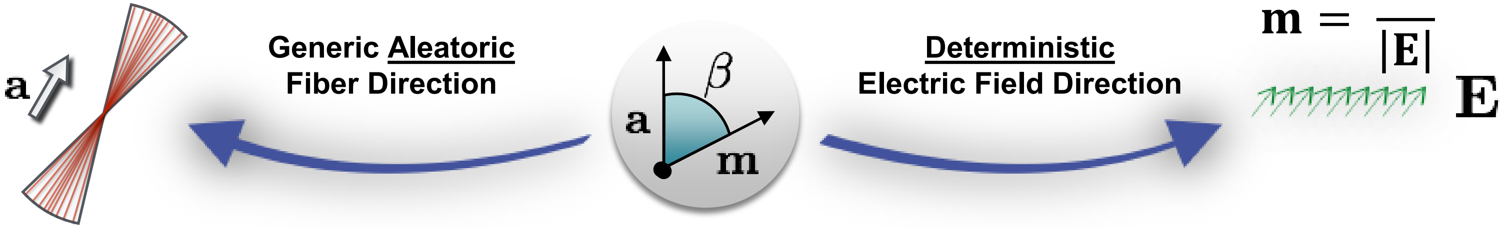

$$\mathbf{m} = \frac{\mathbf{E}}{|\mathbf{E}|}$$

- The active deformation gradient for the fiber distribution is the integral over the unit sphere

$$\mathbf{F}^a = g_1(\mathbf{E})\mathbf{I} + \int_\omega g_2(\mathbf{E})\mathbf{A}\rho(\mathbf{a})d\omega$$

- It retains a deterministic nature, though derived from aleatoric microstructural contributions.

Validation of the material model and predictability

- Validation of the proposed active model against **equi-biaxial tests** on cardiac tissues showing non-zero stress at null strain (experiments **Sommer et al, 2015**, simulations **Pandolfi et al, 2016**)

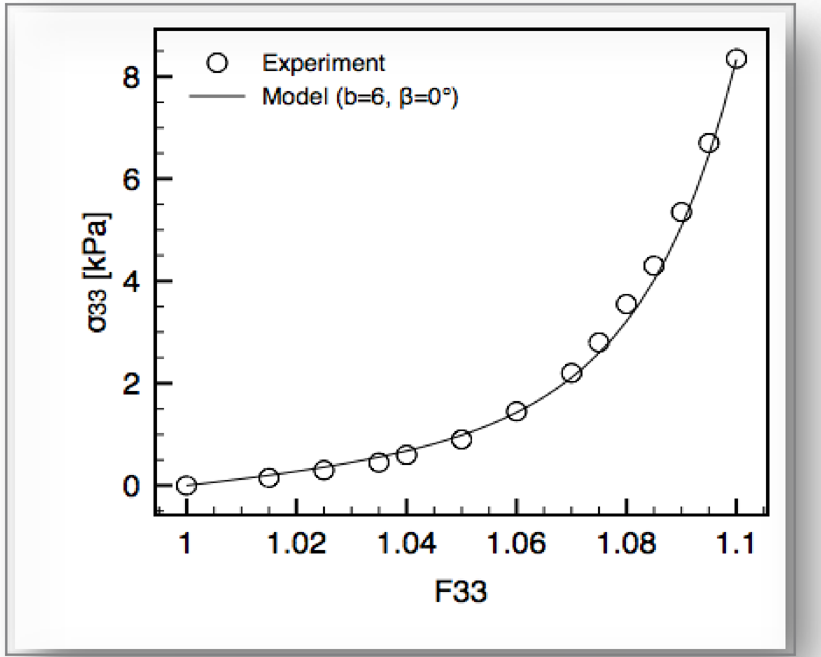

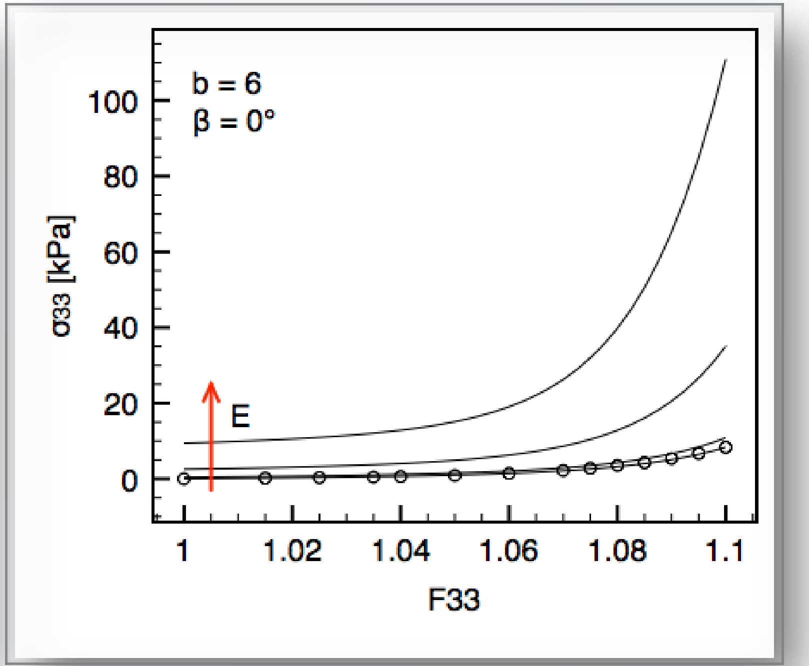

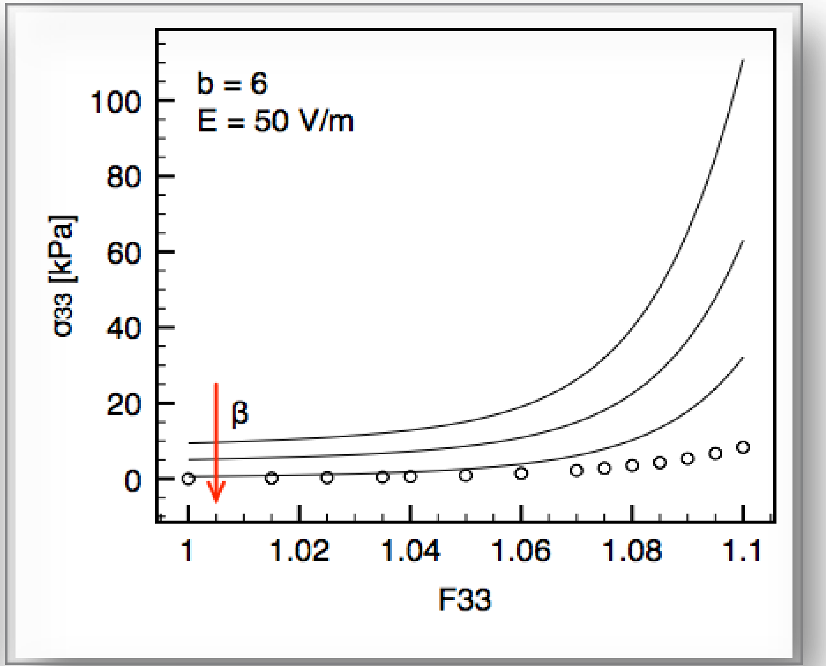

Expected mechanical response (E intensity and angle β with fibers)

Electric field intensity

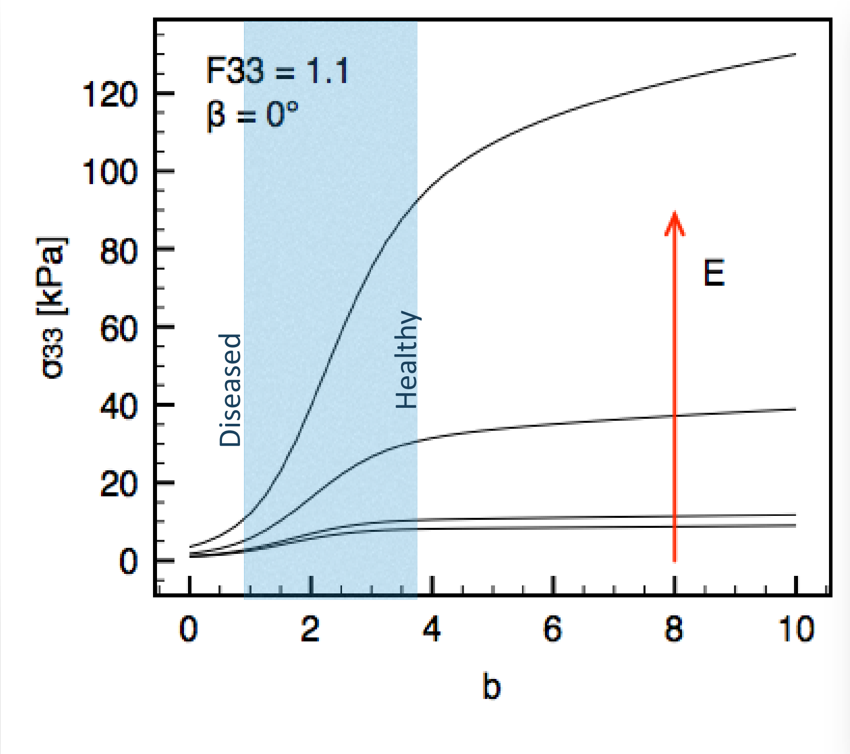

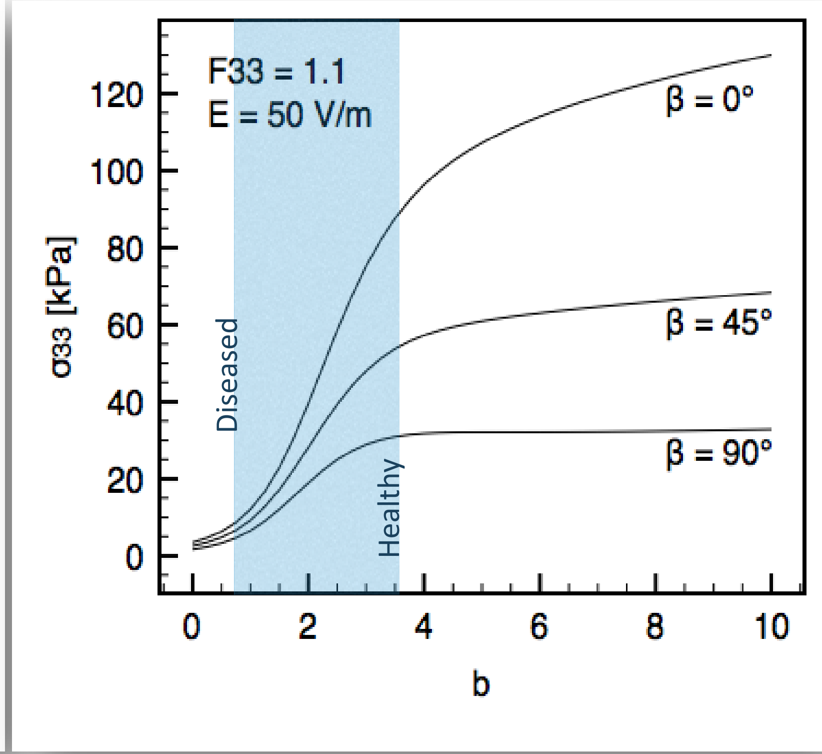

Electric field orientation

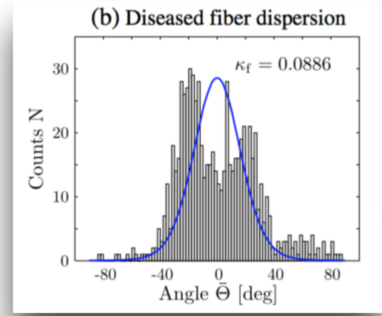

Pandolfi et al, 2013

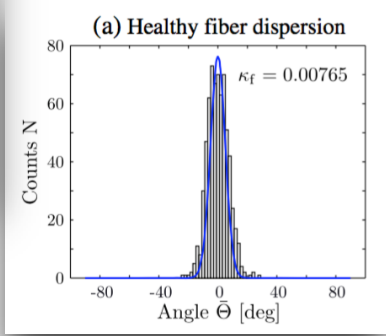

Erikkson et al, 2013

MRI of colon portions – VMTK toolkit

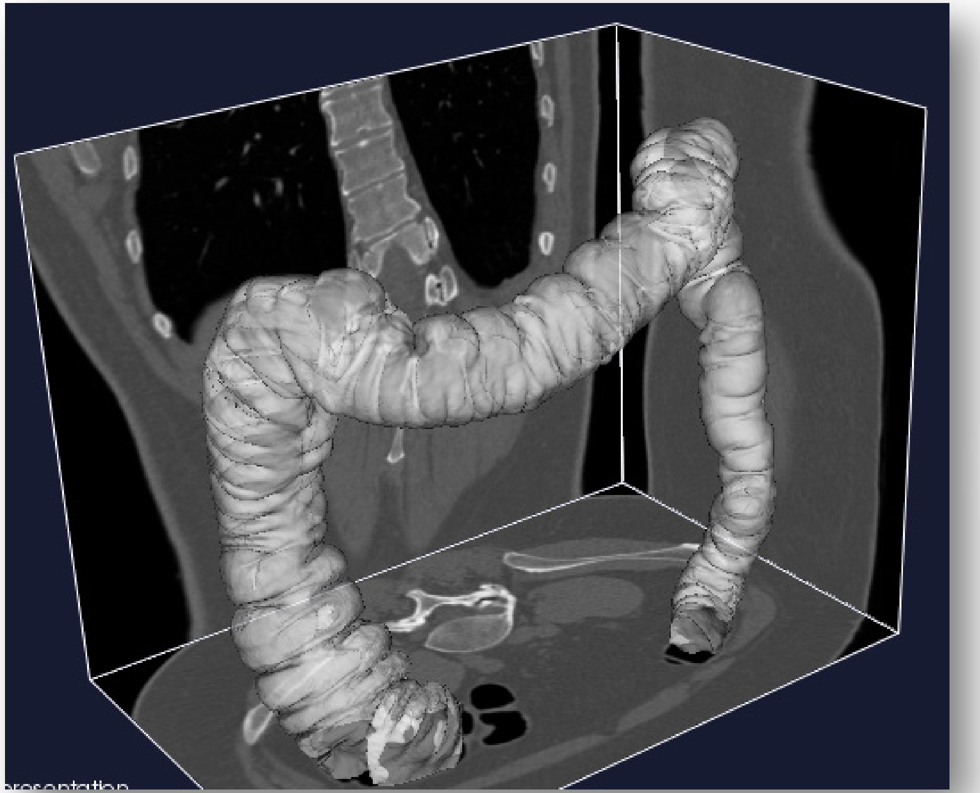

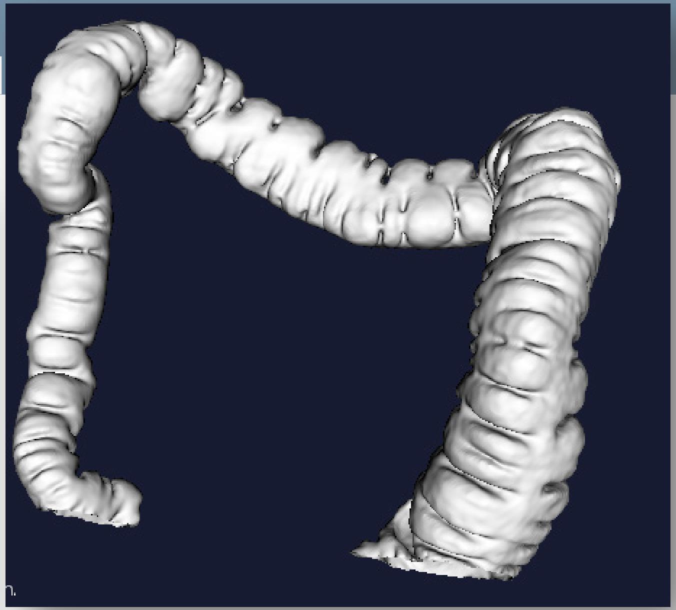

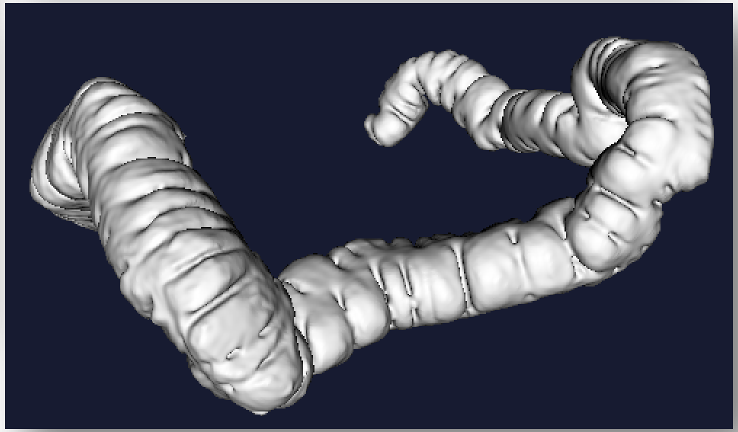

Numerical model and fiber orientation

Computational FE mesh
~ 10K nodes
~ 40K elements

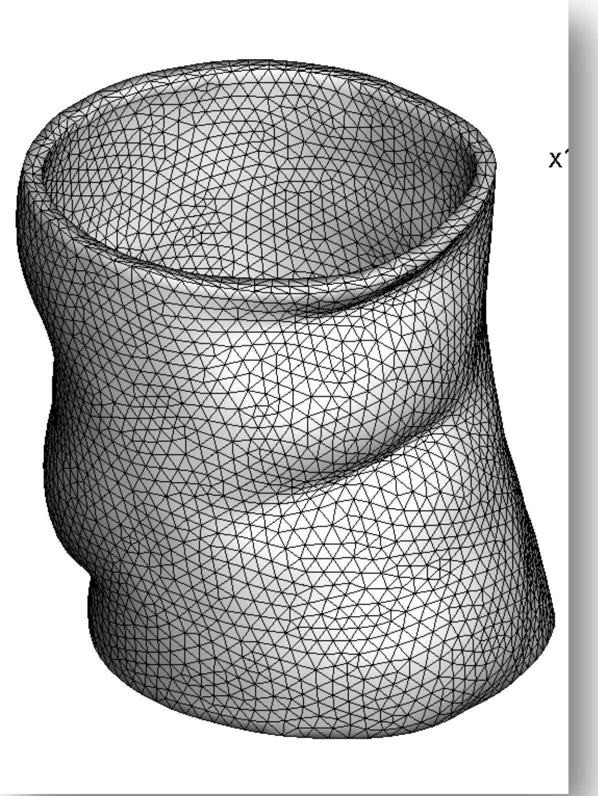

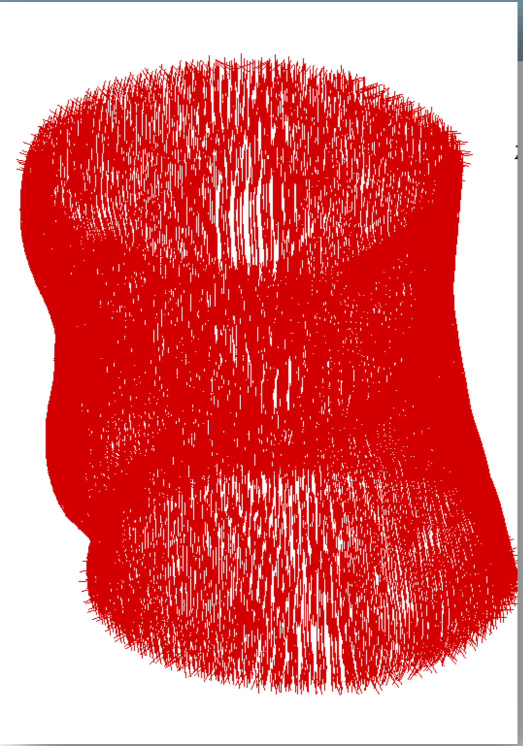

Longitudinal fibers (external)

Circumferential fibers (internal)

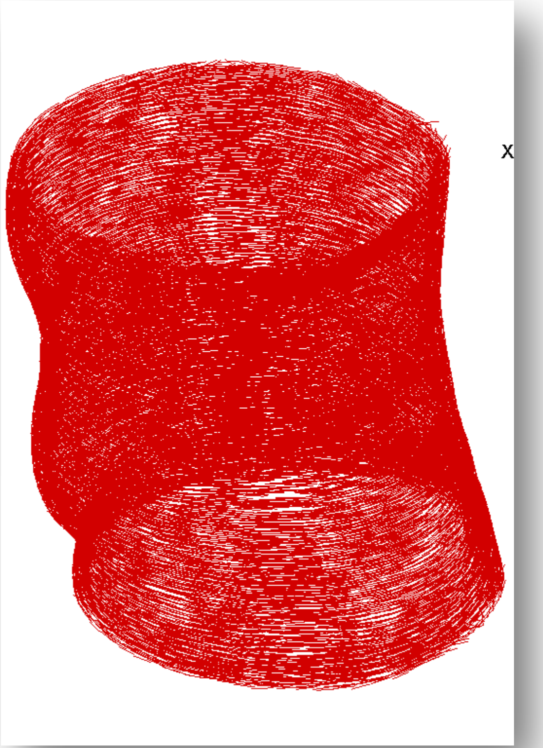

Elastic material properties from literature

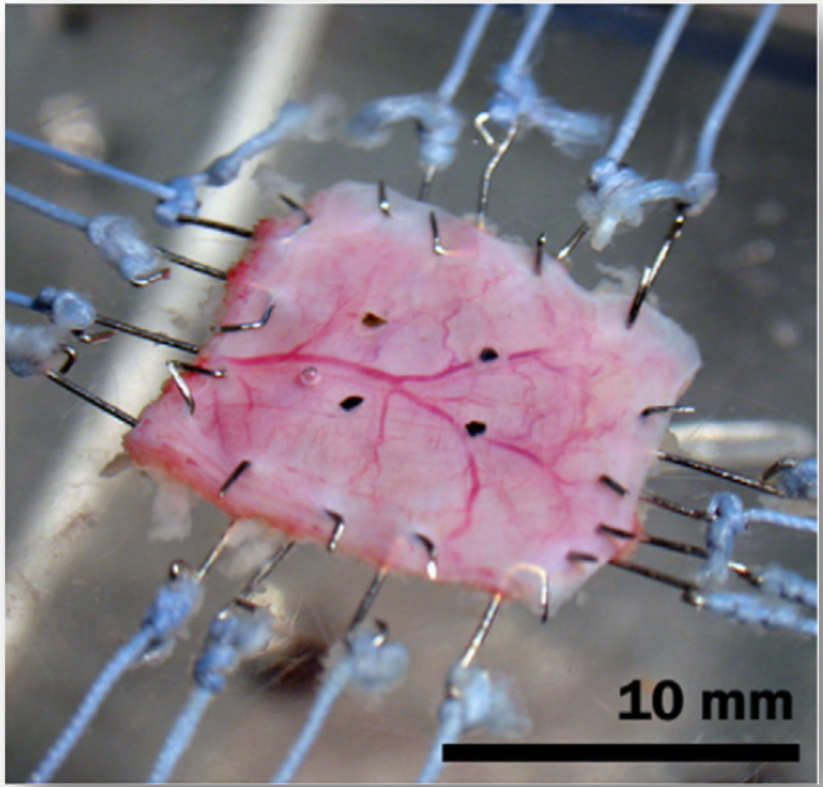

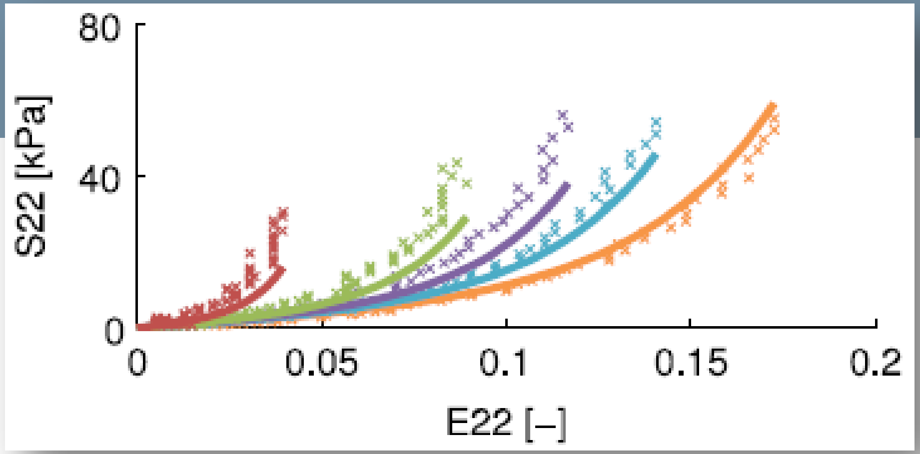

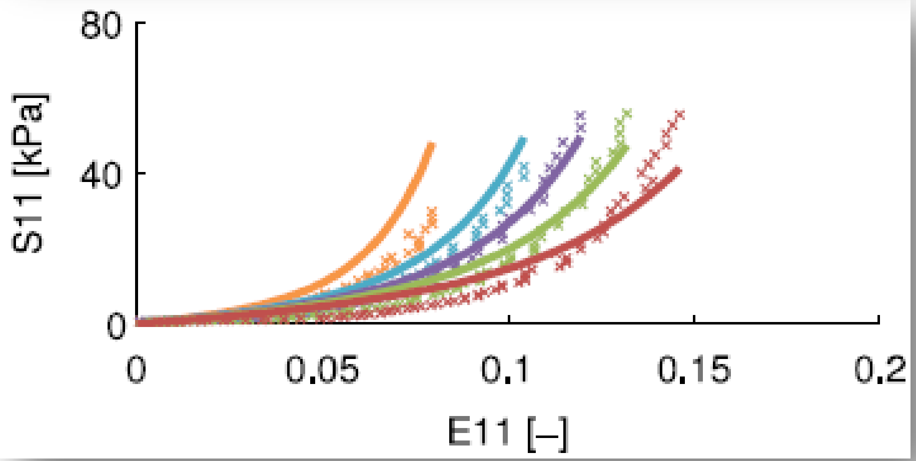

- Experimental data on porcine intestine biaxial test **[Bellini et al., JMBBM 2011]**
- Loaded circumferential (left) and longitudinal directions (right) with different stretch ratio on a portion of jejunum.

Calibration of the passive elasticity

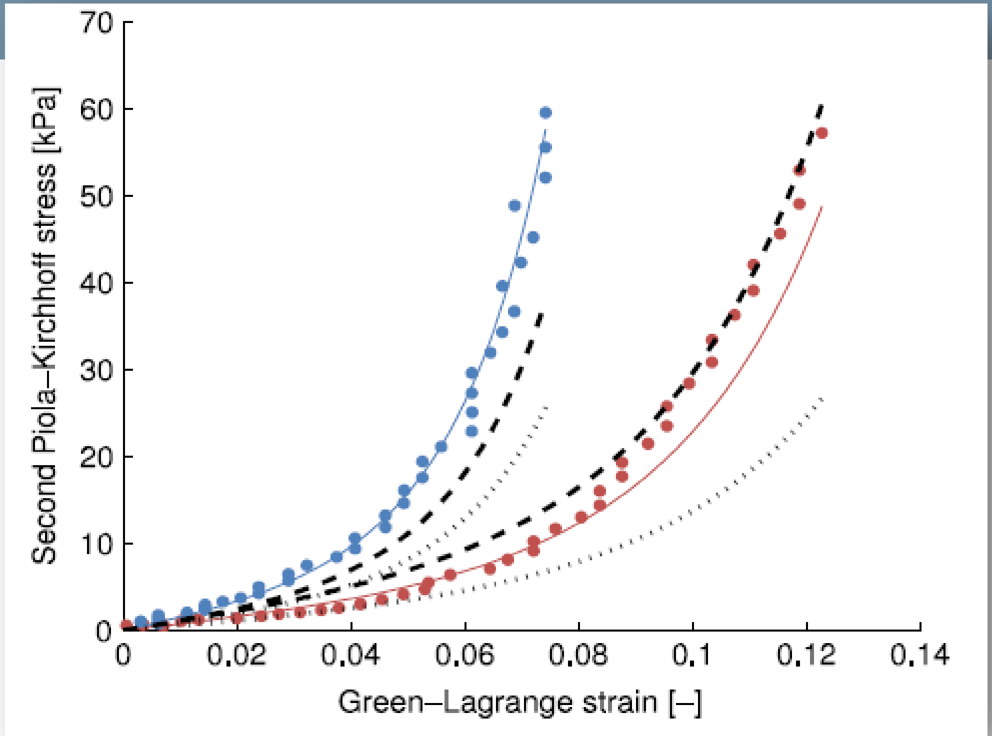

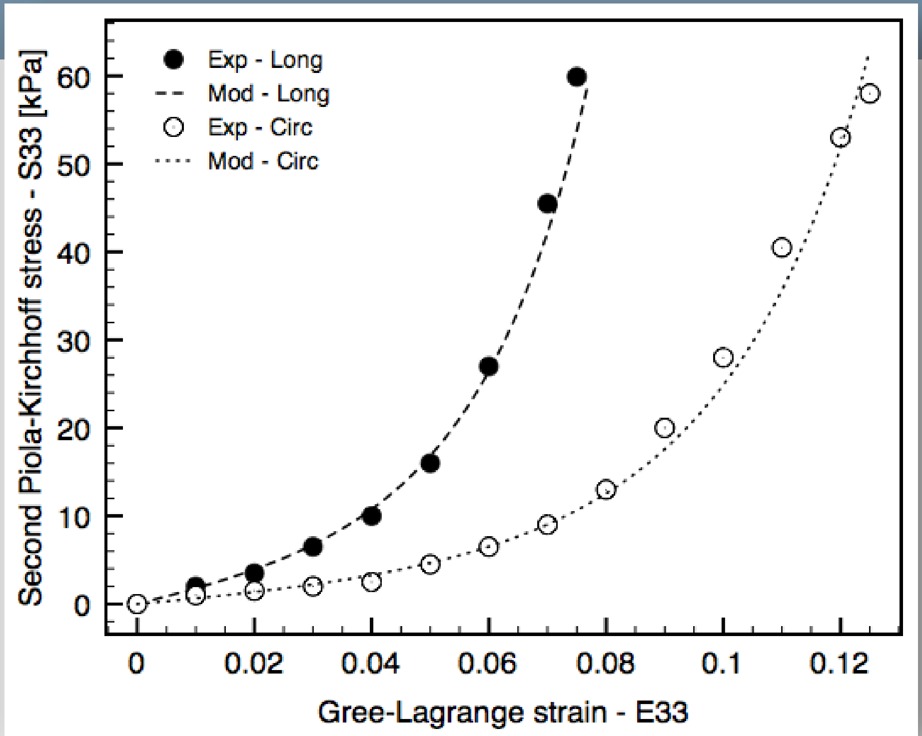

K [kPa]	m_1 [kPa]	m_2 [kPa]	k_4 [kPa]	k_{42} [-]	k_6 [kPa]	k_{62} [-]	z [kPa s]	h [kPa s]
5.5	1.	1.	55.	56.	20.	29.	5.5	1.5

Electro-active simulation

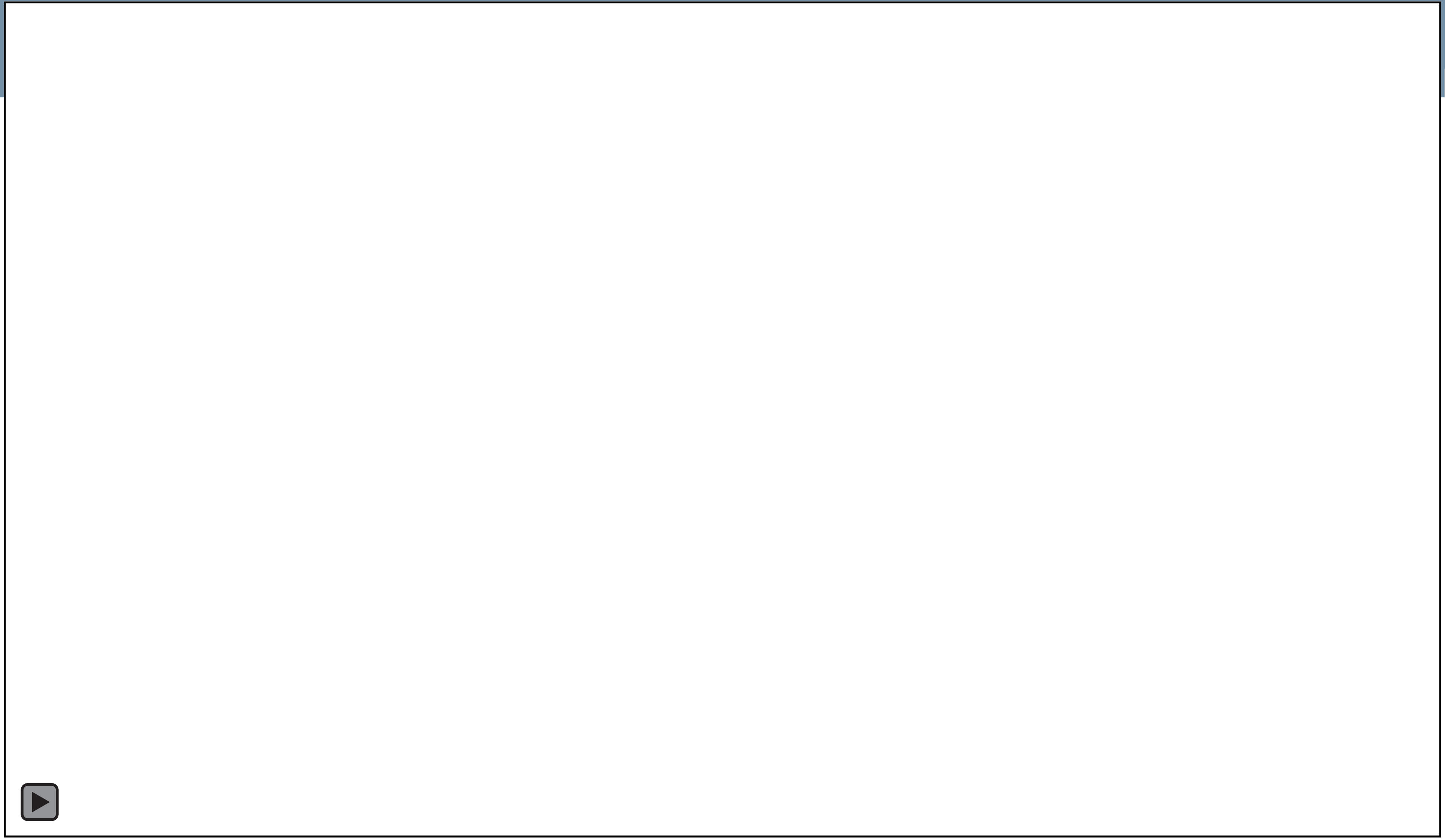

Summary and conclusion

- Coupled problems represent the forefront of modern computational mechanics
- Computational methods require the definition of models and of space/time discretization
- Models include geometry, boundary condition and, especially, materials
- Modelling requires validation against real world data

- Many materials explored with computational methods are characterized by complexity
  - Multiple internal scales
  - Spatial distribution of micro-components (faults, fibers, voids, …) that define a micro-structure
  - Behavior of complex materials differentiate according to the loading
- Validation of complex materials is complex (comparison with multiple tests to assess the correct modelling of the microstructure)
- Validation of coupled models is in general difficult because coupled experiments are hard to be performed and usually only a few data are recorded.